

Journal Pre-proof

Swimming in an ocean of curves: A functional approach to understanding elephant seal habitat use in the Argentine Basin

Nadège Fonvieille, Christophe Guinet, Martin Saraceno,
Baptiste Picard, Martin Tournier, Pauline Goulet, Claudio Campagna,
Julieta Campagna, David Nerini



PII: S0079-6611(23)00163-5
DOI: <https://doi.org/10.1016/j.pocean.2023.103120>
Reference: PROOCE 103120

To appear in: *Progress in Oceanography*

Received date: 6 March 2023
Revised date: 30 June 2023
Accepted date: 5 September 2023

Please cite this article as: N. Fonvieille, C. Guinet, M. Saraceno et al., Swimming in an ocean of curves: A functional approach to understanding elephant seal habitat use in the Argentine Basin. *Progress in Oceanography* (2023), doi: <https://doi.org/10.1016/j.pocean.2023.103120>.

This is a PDF file of an article that has undergone enhancements after acceptance, such as the addition of a cover page and metadata, and formatting for readability, but it is not yet the definitive version of record. This version will undergo additional copyediting, typesetting and review before it is published in its final form, but we are providing this version to give early visibility of the article. Please note that, during the production process, errors may be discovered which could affect the content, and all legal disclaimers that apply to the journal pertain.

© 2023 Published by Elsevier Ltd.

1
2
3
4
5
6
7
8
9
10
11
12
13
14
15
16
17
18
19
20
21
22
23
24
25
26
27
28
29
30
31
32
33
34
35
36
37
38

Swimming in an ocean of curves: A functional approach to understanding elephant seal habitat use in the Argentine Basin

Nadège Fonvieille^{a,b,*}, Christophe Guinet^b, Martin Saraceno^{c,d}, Baptiste Picard^b, Martin Tournier^b, Pauline Goulet^b, Claudio Campagna^e, Julieta Campagna^f and David Nerini^a

^aMediterranean Institute of Oceanography, Aix Marseille Université, CNRS/INSU, Université de Toulon, IRD, 13288, Marseille cedex 09, France

^bCentre of Biological Studies Chizé (CEBC), Villiers-en-Bois, France

^cCONICET - Universidad de Buenos Aires, Facultad de Ciencias Exactas y Naturales, Departamento de Ciencias de la Atmósfera y los Océanos, Mepukada, Buenos Aires, Argentine

^dCNRS – IRD – CONICET – UBA. Instituto Franco- Argentino para el Estudio del Clima y sus Impactos (UMI 3351 IFAECI), Buenos Aires, Argentina

^eWildlife Conservation Society, Marine and Argentina Programs, Buenos Aires, Argentina

^fCentro para el Estudio de Sistemas Marinos (CESIMAR), CENPAT-CONICET, Puerto Madryn, Argentina

Keywords: Southern elephant seals, Habitat use, Functional analysis, Model-based clustering, Brazil-Malvinas Confluence

39
40
41
42
43
44
45
46
47
48
49
50
51
52
53
54
55
56
57
58
59
60
61
62
63
64
65

Abstract

1
2
3
4
5
6
7
8
9
10
11
12

In recent decades, southern elephant seals (SES) have become a species of particular importance in ocean data acquisition. The scientific community has taken advantage of technological advances coupled with suitable SES biological traits to record numerous variables in challenging environments and to study interactions between SES and oceanographic features. In the context of big dataset acquisition, there is a growing need for methodological tools to analyze and extract key data features while integrating their complexity. Although much attention has been paid to study elephant seal foraging strategies, the continuity of their surrounding three-dimensional environments is seldom integrated. Knowledge gaps persist in understanding habitat use by SES, while the representativeness of a predator-based approach to understanding ecosys-

tem structuring is still questioned. In this study, we explore SES habitat use by using a functional data analysis approach (FDA) to describe the foraging environment of five female elephant seals feeding in the Southwestern Atlantic Ocean. Functional principal component analysis followed by model-based clustering were applied to temperature and salinity (TS) profiles from Mercator model outputs to discriminate waters sharing similar thermohaline structures. Secondly, in situ TS profiles recorded by the SES were employed to determine the habitat visited within the range of potential environments identified from the model data. Four Functional Oceanographic Domains (FOD) were identified in the Brazil-Malvinas Confluence, all visited, in varying proportion, by four of the five females studied. We found that the females favored areas where all the FODs converge and mix, generating thermal fronts and eddies. Prey-capture attempts increased in such areas. Our results are in accordance with previous findings, suggesting that (sub-)mesoscale features act as biological hotspots. This study highlights the potential of coupling FDA with model-based clustering for describing complex environments with minimal loss of information. As well as contributing to better understanding of elephant seal habitat use and foraging strategies, this approach opens up a wide range of applications in oceanography and ecology.

1 Introduction

Bio-logging is defined as the use of miniaturized animal-borne devices that provide data on animal movement, behavior, physiology or environment. Bio-loggers were first developed to investigate the at-sea behavior and distribution of enigmatic marine megafauna (Block et al., 2011; Boehme et al., 2012; Hays et al., 2016; Hussey et al., 2015; Jonsen et al., 2007; Payne et al., 2018). Nowadays, a wide range of small-size instruments is available to sample, at high frequency, fine-scale foraging behavior along encountered oceanographic conditions (Block et al., 2016; Evans et al., 2013; Fedak et al., 2004; Guinet et al., 2014; Harcourt et al., 2019). Large marine mammals, especially pinnipeds, have become species of particular importance in marine-environment data acquisition through bio-logging approaches (Bailleul et al., 2015; Fedak, 2013; Hindell et al., 2020; March et al., 2020; Roquet et al., 2013). In this context, southern elephant seals (*Mirounga leonina*, Linnaeus 1758, SES hereafter)

45 may currently represent the most significant marine animal contribution towards the
46 collection of in situ oceanographic data. For instance, two-thirds of the temperature
47 and salinity profiles available for the Southern Ocean are provided by SES equipped
48 with Satellite Relay Data Loggers-CTD (SRDL-CTD) as part of the AniBOS network
49 within the Global Ocean Observing System (McMahon et al., 2021; Roquet et al.,
50 2014).

51 The most commonly-monitored environmental variables include physical (temper-
52 ature, salinity, light), bio-geochemical (chlorophyll-*a*, oxygen) as well as biological
53 variables such as bioluminescence (Bailleul et al., 2015; Guinet et al., 2014; Jaud et
54 al., 2012; Vacquie-Garcia et al., 2012). More recently, the assessment of mid-trophic
55 level organisms including SES preys, ranging in size from a few millimeters to a few
56 centimeters, was made possible by implementing a miniature echo-sounding device
57 (Goulet et al., 2019; Tournier et al., 2021). SES behavior information includes at-sea
58 locations, fine-scale three-dimensional (3D) diving behavior, swimming effort, as well
59 as prey-capture attempts (PCA, Le Bras et al., 2017; Le Bras et al., 2016). These
60 technological advances have led to substantial multivariate environmental and behav-
61 ioral datasets used by physicists to investigate fine-scale processes (Aubone et al.,
62 2021; Carse et al., 2015; Roquet et al., 2013), and biologists to study the at-sea ecol-
63 ogy of these marine predators, thus revealing critical foraging habitats (Labrousse et
64 al., 2018) and providing key information on the distribution and accessibility of food
65 resources (Goulet et al., 2019; Tournier et al., 2021). Finally, combining SES foraging
66 behavior with oceanographic conditions encountered along an animal's trajectory is
67 useful for understanding the trophic web structure and for studying organisms in re-
68 lation to key physical processes (Bailleul et al., 2010; Cotté et al., 2015; Della Penna
69 et al., 2015; Dragon et al., 2010; Rivière et al., 2019).

70 However, such a predator-based approach also has its limitations. The specific behav-
71 ior of individual animals may induce selective bias of the sampled in situ environmen-
72 tal conditions (Conn et al., 2017; Dinsdale and Salibian-Barrera, 2019). Therefore,
73 SES bio-sampling may not be suited for monitoring the full range of oceanographic
74 conditions available to these animals. Consequently, it can be critical to consider
75 the visited habitats as only part of a realm of possibilities when assessing the forag-
76 ing habitat targeted by these predators. Although some species can reasonably be
77 assumed to be mainly constrained by surface environmental conditions, like surface-

78 feeding seabirds (Schreer and Kovacs, 1997), diving species evolve in different layers of
79 the water column. SES are deep divers (Hindell et al., 2016), and as such, one major
80 difficulty when studying their foraging behavior is positioning it within a broader 3D
81 oceanographic context. Satellite oceanographic data, while helpful for comparing ma-
82 rine predator tracks with sea surface temperature, salinity, sea surface height and/or
83 ocean colors, cannot inform on the vertical variations of oceanographic conditions.
84 Yet, for an equal distance, vertical gradients of physicochemical variables are much
85 more accentuated than oceanographic gradients at the surface (Wunsch and Ferrari,
86 2004). Therefore, when investigating the foraging behavior of (deep) diving preda-
87 tors, it is crucial to contextualize this behavior in a 3D oceanographic environment.
88 In this study, we aim to understand the habitat used by elephant seals by analyzing
89 the 3D habitat visited in relation to oceanographic conditions at a regional scale.

90 Previous studies using classic oceanographic features tend to summarize the structure
91 of the whole water column by a single discrete value like mean temperature or tempera-
92 ture at a given depth (Guinet et al., 2014; Hindell et al., 2016). However, tempera-
93 ture and salinity (hereafter TS) profiles are sampled by SES with SRDL-CTD (0.5 Hz
94 frequency) which provide a considerable dataset over an animal's trip. Reducing these
95 high-resolution profiles to single discrete descriptors leads to a substantial loss of in-
96 formation. Functional data analysis (FDA), first introduced by Ramsay (1982), allows
97 manipulating curves or functions rather than scalars or vectors (discrete measures)
98 used in classic data-analysis techniques (Ramsay and Silverman, 2005). Functional
99 approaches encompass numerous methods and offer a wide range of applications in
100 various fields of sciences (Cuevas, 2014; Ullah and Finch, 2013; Wang et al., 2016).
101 This statistical framework has recently been applied in marine science and showed
102 strong potential for describing vertical oceanographic features at a global scale (Pau-
103 thenet et al., 2017; Pauthenet et al., 2019). It is well suited to modeling TS profiles
104 that are continuous variable functions of depth and can be applied to either in situ or
105 modeled data without being affected by the sampling grid. Alongside FDA, various
106 studies have proposed using profile classification models (PCM, Maze, Mercier, and
107 Cabanes, 2017) to identify oceanographic regimes (Boehme and Rosso, 2021; Jones
108 et al., 2019; Maze, Mercier, Fablet, et al., 2017; Rosso et al., 2020). PCMs take
109 advantage of Gaussian mixture modeling (GMM) to find meaningful objective groups
110 in data (Bouveyron et al., 2019). Yet, while these studies use temperature and/or

111 salinity profiles, they do not employ functional data methodology.

112 In this study, we propose to combine FDA with model-based clustering within a col-
113 lection of temperature and salinity profiles. The proposed method shows promising
114 results, allowing the identification of spatio-temporal-coherent oceanographic regimes
115 sharing similar vertical thermohaline structures, named hereafter Functional Oceanographic
116 Domains (FOD). Another originality of this paper resides in the coupling
117 of TS profiles from Mercator model outputs and from head-mounted SES loggers.
118 Profiles from the model are used to describe the vertical thermohaline oceanographic
119 environment at a regional scale and identify FODs, while in situ profiles are used to
120 determine the actual conditions visited by the SES within the range of possibilities
121 provided by the model. This research offers new insights into the bias induced by
122 SES choices in the representativeness of sampled environmental conditions. More-
123 over, prey-capture rates are analyzed to understand the impacts of oceanographic
124 conditions on SES foraging strategies. This study is conducted on the Patagonian
125 (Argentina) SES population known to forage within the Brazil-Malvinas Confluence
126 (BMC), a region of major importance for that SES population (Campagna et al.,
127 2021).

128 2 Method

129 2.1 Study area

130 The study is carried out on recently acquired data collected by SES breeding in
131 southern Argentina (Península Valdés, 42°57' S, 63°59' W) and mainly feeding in
132 the Southwestern Atlantic Ocean (Campagna et al., 2006; Campagna et al., 2021).
133 This region includes the meeting zone between the Brazilian Current (BC) and the
134 Malvinas Current (MC). The MC finds its origin in the Antarctic Circumpolar Cur-
135 rent (ACC) that flows eastward around Antarctica (Piola and Gordon, 1989). After
136 passing the Drake Passage, south of the Patagonian shelf, a portion of the northern
137 branch of the ACC is deflected northward, crossing the North Scotia Ridge mainly
138 through the eastern and western flanks of the Burdwood Bank and the Shag Rocks
139 Passage (Artana et al., 2016) and giving origin to the MC. Rounding east of the
140 Falklands (Malvinas) Islands, the MC finds a way northward along the continental

141 slope, following isopotential vorticity contours (Saraceno et al., 2004) and carrying
142 cold and nutrient-rich subantarctic waters. Contoured by the Subantarctic Front
143 (SAF), the MC collides with the BC, flowing southward along the Brazil coast at \sim
144 38° S (Gordon, 1981; Saraceno et al., 2004). The collision generates a thermohaline
145 front called the Brazil-Malvinas Confluence zone (Deacon, 1937). The BMC creates
146 instabilities generating prominent (sub-)mesoscale structures, including eddies, mak-
147 ing the Southwestern Atlantic one of the most energetic regions of the world ocean
148 (Chelton et al., 1990).

149 The focus area is defined by the black rectangle displayed in Figure 1. This area
150 covers the SES post-breeding trajectories in 2018 and 2019 and includes the BMC
151 region. Land covers 9 % of the area. Within the ocean zone, 30 % is shallower than
152 200 meters and corresponds to the Patagonian Continental Shelf (Piola and Falabella,
153 2009). The continental slope ends at 6 000 meters depth, marking the beginning of
154 the Argentine Abyssal Plain also named the Argentine Basin. The GEBCO14 grid is
155 used to define the bathymetry in the area (30 arc second resolution; distributed by
156 the British Oceanographic Data Centre; Weatherall et al., 2015).

157 2.2 Functional analysis

158 A bivariate principal component analysis for functional data (FPCA, functional prin-
159 cipal component analysis) is performed on temperature and salinity (TS) profiles from
160 Mercator model outputs to describe the vertical structure of the BMC area and ex-
161 tract the principal modes of variability at the regional scale. Model-based clustering
162 is applied on the first principal components (PC) of the FPCA to define regimes shar-
163 ing similar water properties, the Functional Oceanographic Domains (FOD). In situ
164 TS profiles recorded by five female southern elephant seals (SES) are then projected
165 onto the factorial map of the model-derived FPCA in order to assign each SES dive to
166 one FOD. This step gained information on the oceanographic regimes visited by each
167 female along her trajectory. Figure 2 summarizes the different steps of the method.
168 All analyses are conducted in R (Team, 2021) and with Matlab R2021b.

169 2.2.1 Datasets

170 *Profiles from elephant seal dives*

171 Nine post-breeding female SES were tagged in october 2018 with different bio-loggers
172 at Península Valdés, following the procedure described in McMahon et al. (2008).
173 The females were captured and anesthetized with an intravenous injection of Zo-
174 letil®100 (1:1 combination of tiletamine and zolazepam) and tags were glued to the
175 pelage using Araldite adhesive. The animal manipulations were in accordance with
176 the “Use of Animals for Scientific Reasons (APAFIS)” ethics committee guidelines.
177 Among phocids, the elephant seal is a particularly well-suited species for monitoring
178 the oceans. It forages over extended distances (thousands of kilometers), diving con-
179 tinuously (i.e. 60 times a day) at depths generally ranging between 400 and 1 000
180 meters, and exceptionally up to 2 000 meters (Hindell et al., 2016). SES return to
181 land to breed and molt at predictable cycles and places, facilitating device recovery
182 and high-frequency data acquisition. Their large size allows scientists to equip them
183 with several multi-sensor loggers with minimal disturbance (McMahon et al., 2008).
184 All individuals were equipped with a SRDL-CTD tag (Sea Mammal Research Unit,
185 St Andrews, UK). The depth was logged with a 0.5 Hz frequency and 0.5 m resolu-
186 tion. A dive corresponds to a period during which the animal is deeper than 15 m
187 continuously for at least 300 s (Le Bras et al., 2016). Each dive is associated with
188 one temperature and one salinity profile, sampled and corrected from the ascending
189 phase of the dive (Roquet et al., 2011; Siegelman et al., 2019). The CTD tag provides
190 discrete TS measurements with a 0.5 Hz frequency and a 0.01 °C and 0.03 psu accu-
191 racy. Locations of the dives were recorded using a Global Positioning System (GPS)
192 for four individuals equipped with a micro-sonar or a DTAG (Goulet et al., 2020;
193 Goulet et al., 2019). The (approximately) 20 m resolution provided by the GPS of-
194 fers accurate coordinates but its short battery lifetime led to non-localized TS profiles
195 as the CTD continued to record data after the GPS stopped. Argos locations (2-10
196 km resolution; Lopez et al., 2015) provided by head-mounted SRDL-CTD or SPOT
197 tags (Wildlife Computers, USA) were used to obtain dive coordinates for the other
198 five SES. Head-mounted accelerometer sensors included in the SRDL-CTD, sonar and
199 DTAGs are used to assess prey-capture attempts (PCA, Gallon et al., 2013; Viviant
200 et al., 2010). The prey-capture rate (i.e. PCAs per unit time, referred to as PCR) is
201 calculated from the dive duration (Guinet et al., 2014; Jouma’a et al., 2016) and used
202 as a proxy of foraging performances. A day-night period is assigned to all localized
203 dives based on the sun angle (Guinet et al., 2014). Day periods are defined when the

204 sun angle is $> 12^\circ$ above the horizon, while night periods are determined as $< -12^\circ$
205 below the horizon. The threshold of 12° is selected to ensure a clear distinction from
206 dives occurring during the twilight period.

207 Out of the nine SES equipped, only five foraging within the BMC are kept for the
208 present study (Figure 1). Among the discarded individuals, one of the nine females
209 traveled southward, following the coast of Argentina to Chile, and two others spent
210 the whole trip foraging over the Patagonian slope. A fourth female presenting out-of-
211 range salinity data was also excluded. Those incorrect data were detected as outliers
212 via the FCPA described in Section 2.2.3. To determine oceanographic conditions
213 visited by the five selected SES, all localized and non-localized TS profiles deeper
214 than 450 m are considered, accounting for a total of 9 537 dives. These recorded
215 profiles constitute the in situ dataset used in this work (step 1 Figure 2).

216 *Profiles from Mercator model outputs*

217 The general three-dimensional oceanographic temperature and salinity context of
218 the study area is obtained by the GLORYS12V1 product provided by the Coper-
219 nicus Marine Environment Monitoring Service (CMEMS, [https://doi.org/10.48670/
220 moi-00021](https://doi.org/10.48670/moi-00021)). The dataset used to define the environmental conditions, referred to
221 as model-derived profiles, corresponds to daily averaged TS profiles covering the de-
222 fined area (Figure 1) from October 21, 2018, to January 23, 2019, spanning a total
223 of 95 days. The horizontal resolution of the dataset is $1/12^\circ$, which corresponds to
224 approximately 8 km. The output products are displayed on a 193×133 horizontal
225 grid (longitude \times latitude) and 50 vertical irregular depth levels extended from 0.5
226 m (surface) to 5 728 m (bottom). Considering that the depth reached by the in situ
227 profiles depends on the SES behavior, it was decided that statistical analysis would be
228 applied on profiles (model and in situ) between 20 m and 450 m. This choice excludes
229 profiles sampled on the Patagonian continental shelf (< 200 m) while capturing most
230 of the vertical variability in the open ocean and retaining a large proportion of in
231 situ profiles. The discrete model-derived profiles are linearly interpolated in order to
232 obtain a uniform vertical grid with 44×10 m levels from 20 to 450 m. This step al-
233 lows avoidance of spurious bumpiness in curve fitting (Pauthenet et al., 2019). Those
234 profiles constitute the model-derived dataset used in this work (step 1 Figure 2).

235 2.2.2 TS profiles as continuous curves

1 236 Temperature and salinity profiles are continuous functions along depth. These data
 2 237 are always available as discrete values, induced by the sampling method. Yet, values
 3
 4 238 within a profile $x(t)$ are ordered based on the parameter t . This link between two
 5
 6 239 consecutive values implies particular considerations. First developed by Ramsay and
 7
 8 240 Silverman (2005), statistical functional methods are explicitly designed to process
 9
 10 241 and study data that are functions, considering one curve as a single entity. Each SES
 11
 12 242 dive or each pixel (i.e. model-derived data) is described by two profiles (temperature
 13
 14 243 and salinity), making the data bivariate functions. Those two profiles are intrinsically
 15
 16 244 linked and regarded as a unique observation.

17
 18 245 The first stage of the functional data analysis (step 1 to 2 Figure 2) is to transform
 19
 20 246 the discrete TS profiles into functions $x(z)$, with $z \in [20; 450]$ being the depth in
 21
 22 247 meters (library `fda`, Ramsay et al., 2009). This step is achieved by decomposing the
 23
 24 248 profiles on a cubic B-spline basis (Wahba, 1990). Each profile n is expressed as a
 25
 26 249 linear combination of basis functions $\phi_k(z)$:

$$27 \quad x_n^i(z) = \sum_{k=1}^K \alpha_{n,k}^i \phi_k(z), \quad i \in \{T, S\}, \quad n = 1, \dots, N, \quad (1)$$

28
 29
 30
 31
 32
 33
 34 250 where the $\alpha_{n,k}^i$ coefficients are estimated by penalized least squares regression (see
 35
 36 251 Supplementary Material) and N is the number of profiles. The number K of basis
 37
 38 252 functions controls the vertical smoothness. Both model-derived and in situ profiles
 39
 40 253 are expressed according to the same basis to facilitate their comparison. As the
 41
 42 254 model-derived dataset used in this study is composed of more than 2×1.5 million
 43
 44 255 profiles (T and S profiles) with 44 values per profile, one goal of the decomposition
 45
 46 256 procedure is to reduce the dimension of the data. A basis of $K = 15$ functions is
 47
 48 257 chosen, allowing sufficient vertical complexity to be kept for both kinds of profiles
 49
 50 258 while summarizing the data with a small number of coefficients (see Supplementary
 51
 52 259 Material). Henceforth, each observation n , consisting of two profiles ($x_n^T(z), x_n^S(z)$),
 53
 54 260 can be expressed as a vector α_n of dimension $2 \times K$, merging temperature and salinity
 55
 56 261 coefficients:

$$57 \quad \alpha_n = (\alpha_{n,1}^T, \dots, \alpha_{n,K}^T ; \alpha_{n,1}^S, \dots, \alpha_{n,K}^S)'. \quad (2)$$

58
 59 262 Model-derived coefficients are stored in a matrix \mathbf{X}_N of size $N \times 2K$, with N the
 60
 61
 62
 63
 64
 65

263 number of model-derived observations (step 2 [Figure 2](#)). The mean model-derived
 264 observation $\bar{\alpha} = (\bar{\alpha}_1^T, \dots, \bar{\alpha}_K^T; \bar{\alpha}_1^S, \dots, \bar{\alpha}_K^S)'$ is evaluated with $\bar{\alpha}_k^i, i \in \{T, S\}, k = 1, \dots, K$,
 265 the empirical mean of the N coefficients k .

266 2.2.3 Functional Oceanographic Domains (FOD)

267 *Functional Principal Component Analysis*

268 Functional principal component analysis (FPCA) is a powerful method to reduce the
 269 dimension of the data (Wang et al., [2016](#)). It decomposes the thermohaline structure
 270 into modes of variability, allowing simultaneous analysis of the shape variation of
 271 temperature and salinity profiles. The search for the main modes of variability is
 272 achieved by solving the following eigenvalue problem:

$$21 \quad \mathbf{VWM} \mathbf{b}_l = \lambda_l \mathbf{b}_l, \quad (3)$$

273 associating \mathbf{b}_l , the l^{th} eigenvector with the λ_l eigenvalue. This step allows us to find
 274 the unique decomposition of the matrix \mathbf{VWM} . The block-structured covariance matrix
 275 \mathbf{V} is computed from the matrix \mathbf{C} of centered coefficients such as $\mathbf{V} = 1/N \times \mathbf{C}'\mathbf{C}$.
 276 The centered matrix \mathbf{C} is obtained by subtracting the coefficients of the average profile
 277 $\bar{\alpha}$ from each row of \mathbf{X}_N . Matrix \mathbf{W} , of size $2K \times 2K$, guarantees the metric
 278 equivalence between the functional problem (working on functions) and its discrete
 279 version (working on coefficients). \mathbf{M} is the weighting matrix used to normalize the coefficients
 280 of temperature and salinity (see Supplementary Material). Each eigenvector
 281 generates two eigenfunctions (ξ_l^T, ξ_l^S) , also called vertical modes (see more details in
 282 Supplementary Material and Pauthenet et al., [2017](#)). A total of $2K$ eigenvectors are
 283 obtained, that can be sorted in ascending order according to their associated eigenvalues.
 284 The eigenvector associated with the largest eigenvalue corresponds to the first
 285 vertical mode. The main factors of variability can be seen as a perturbation of the
 286 mean function (\bar{x}^T, \bar{x}^S) by adding or subtracting the eigenfunctions (ξ_l^T, ξ_l^S) :

$$53 \quad \bar{x}^i \pm \sqrt{\lambda_l} \xi_l^i, i \in \{T, S\}. \quad (4)$$

287 The FPCA is realized with the model-derived TS profiles (step 3 [Figure 2](#)). The
 288 observations can be projected into a 2D map using the first two principal components

289 (PC) computed as: $\mathbf{c}_l = \mathbf{C}\mathbf{M}^{-1/2}\mathbf{W}^{-1/2}\mathbf{b}_l, l = 1, 2$. PCs are the uncorrelated linear
 290 combinations of the original variables. They capture the variance of the system. For
 291 more details on the bivariate FPCA procedure, the reader is referred to Nerini et al.
 292 (2022) and Pauthenet et al. (2017).

293 *Model-based clustering*

294 Oceanographic regimes are identified using model-based clustering (library `mclust`,
 295 Scrucca et al., 2016). First introduced by Wolfe in 1963, model-based clustering
 296 is a clustering method based on a probability model defined by a finite mixture of
 297 multivariate Gaussian distributions, called components. The probability distribution
 298 of the P -variate observation $\mathbf{y}_n = (c_{n,1}, \dots, c_{n,P})'$, can be seen as a weighted average
 299 of G conditional probability functions f_g , G being the number of components:

$$p(\mathbf{y}_n) = \sum_{g=1}^G \tau_g f_g(\mathbf{y}_n | \boldsymbol{\mu}_g, \boldsymbol{\Sigma}_g). \quad (5)$$

300 The parameter τ_g is the probability that an observation was generated by the g^{th}
 301 component while $\boldsymbol{\mu}_g$ and $\boldsymbol{\Sigma}_g$ are parameters that control the shape of f_g . The method
 302 allows us to assess uncertainty about the clustering. Each cluster found is modeled
 303 by its own probability distribution. As commonly used, the function f_g is chosen as
 304 a multivariate normal density ϕ_g :

$$\phi_g(\mathbf{y}_n | \boldsymbol{\mu}_g, \boldsymbol{\Sigma}_g) = \frac{\exp(-\frac{1}{2}(\mathbf{y}_n - \boldsymbol{\mu}_g)' \boldsymbol{\Sigma}_g^{-1} (\mathbf{y}_n - \boldsymbol{\mu}_g))}{(2\pi)^{P/2} |\boldsymbol{\Sigma}_g|^{1/2}}, \quad (6)$$

305 where P is the size of the vector \mathbf{y}_n , and the parameters $\boldsymbol{\mu}_g$ and $\boldsymbol{\Sigma}_g$ correspond
 306 respectively to the mean vector and the covariance matrix of the Gaussian density
 307 ϕ_g . The model potentially owns a large number of parameters, depending on the
 308 dimension and the number of groups, which may lead to computational issues in
 309 the estimation process. A common way use to address this problem is to control the
 310 geometric properties of the mixture components, known as Volume-Shape-Orientation
 311 decomposition. Details on the principle are found in Bouveyron et al. (2019). In
 312 order to give as much freedom as possible to the model computation, neither volume,
 313 shape nor orientation were constrained to be equal across the clusters. The choice
 314 of this model, identified by the letters VVV (for varying geometry), is in agreement
 315 with the Bayesian Information Criterion (BIC, Schwarz, 1978) and the Integrated

316 Completed Likelihood (ICL, Biernacki et al., 2000), showing the VVV model as the
317 best combination.

1
2
3 318 The model-based clustering is applied in the space of the principal components ob-
4
5 319 tained from the model-derived FPCA developed above (step 3 Figure 2). The expect-
6
7 320 tation maximization algorithm (Fraley and Raftery, 2002) estimates the parameters
8
9 321 of the model (Equation 6). The most appropriate number of group G is found using
10
11 322 the ICL criterion which is recommended when the focus of the mixture analysis is
12
13 323 clustering instead of density estimation (Biernacki et al., 2000). Initial values of the
14
15 324 algorithm are selected by running the hierarchical model-based clustering with the
16
17 325 VVV model (`mclust` package, Bouveyron et al., 2019). However, since model-based
18
19 326 clustering can be sensitive to the initialization, we executed the model 100 times to
20
21 327 choose the optimal pattern and assess the clustering variability.

23 328 2.2.4 FODs visited by the elephant seals

24
25
26 329 In order to study FODs visited by the SES, in situ TS profiles are projected as new ob-
27
28 330 servations onto the factorial plan of the FPCA realized with model-derived data (step
29
30 331 4 Figure 2). In situ TS profiles are first decomposed into T and S coefficients accord-
31
32 332 ing to the procedure explained in Section 2.2.2. The Δ matrix, of size $M \times 2K$ stores
33
34 333 the new coefficients centered with the vector $\bar{\alpha}$ computed from the model-derived
35
36 334 coefficients (see Section 2.2.2). Estimated scores \hat{c}_l of the l^{th} principal component for
37
38 335 the M new observations are computed as follows:

$$40 \quad \hat{c}_l = \Delta \mathbf{M}^{-1/2} \mathbf{W}^{-1/2} \mathbf{b}_l, \quad (7)$$

41
42
43
44 336 with \mathbf{b}_l as the l^{th} eigenvector. The pair $(\hat{c}_{m,1}, \hat{c}_{m,2})$ gives the coordinates of the m^{th}
45
46 337 in situ TS profile on the 2D map obtained from the model-derived FPCA. This
47
48 338 step relates the environmental conditions visited by the seals to the actual range of
49
50 339 possibilities given by the model-derived analysis.

1
2
3
4
5
6
7
8
9
10
11
12
13
14
15
16
17
18
19
20
21
22
23
24
25
26
27
28
29
30
31
32
33
34
35
36
37
38
39
40
41
42
43
44
45
46
47
48
49
50
51
52
53
54
55
56
57
58
59
60
61
62
63
64
65

3 Results

3.1 Vertical modes in the Brazil-Malvinas Confluence

The functional PCA is performed on 1 524 750 model-derived TS profiles covering the defined area (Figure 1) over 95 days (21 October 2018 to 23 January 2019 inclusive).

The time period corresponds to the foraging trips of the studied SES. Only pixels where the bathymetry is deeper than 450 m are kept for the analysis, excluding the continental shelf area.

The first three vertical modes of variability resulting from the FPCA represent 98.77 % of the variance (Table 1). This value is of the same order as those obtained on the Kerguelen Plateau (Pauthenet et al., 2018) and in the Southern Ocean (Pauthenet et al., 2017). The higher modes capture less than 0.5 % of the variability and are not considered in the following analysis. Spatial distributions of the first and second principal components are displayed in Figure 3a and 3b for 21 October 2018. The maps show that while the FPCA is performed independently of location and day information, spatial patterns arise, accounting for temperature and salinity joint features. Ninety-five maps corresponding to each day of the study can be constructed similarly. Figure 3c and 3d represent the deformation of the mean profile associated with the two first modes.

The first mode, associated with the highest eigenvalue, alone summarizes as much as 94.5 % of the variance with an equivalent contribution of temperature and salinity variability. It involves a modification of the whole water column, going from cold and fresh waters unstratified under 100 m with a noticeable thermocline in the subsurface (positive PC1 in pink, Figure 3), to hot and salty waters (negative PC1 in orange, Figure 3). This mode marks a contrast between Subtropical waters transported by the Brazil Current and Subantarctic waters advected by the Malvinas Current, highlighting sharp thermohaline vertical gradients at the confluence (Figure 3a). The second mode (PC2) describes 3.55 % of the variance. High positive PC2 values (blue, Figure 3) present colder and fresher waters between 20 m and 200 m than high negative values (green, Figure 3). The trend reverses under 200 m. The spatial distribution of PC2 reveals mesoscale structures and a high dynamism produced by the meeting of the two currents (Figure 3b). This mode also opposes waters in the heart and at the

371 edges of the BC (dark blue vs green, Figure 3b). From 20 m to 200 m, temperature
372 and salinity are greater at the edges than in the center part of the current. The third
373 mode (see Supplementary Material) captures the seasonal thermocline development
374 in response to surface heating. Figure 4 depicts the daily mean (continuous lines) and
375 associated standard deviation (dashed lines) trends of the three first modes. A high
376 daily standard deviation time series distinguishes the first mode (see y -axis) marked
377 by a decrease between December and January. This decline can be related to the
378 increase of the daily mean of the first component (pink line, Figure 4), indicating
379 an average drop in temperature and salinity (effect of the first eigenfunction on the
380 mean profiles). The daily mean of the second mode shows a decrease in stages over
381 time, with a small daily standard deviation sharing a similar trend with the daily
382 standard deviation of PC1. Even though the third mode represents less than 1 %
383 of the variance (Table 1) its temporal evolution clearly shows a seasonal (spring to
384 summer) increase of the subsurface temperature in the whole area.

385 In addition, a functional PCA is applied to the in situ TS profiles exclusively. The
386 resulting shape decomposition is similar to the modes obtained with profiles from the
387 model (see Supplementary Material) with comparable variance associated to the first
388 modes (Table 1). This in situ FPCA was conducted independently of the model-
389 derived FPCA and serves solely to compare the obtained modes of variability.

390 3.2 Functional Oceanographic Domains (FOD)

391 In order to cluster profiles sharing similar vertical structures in FODs, a model-based
392 clustering is performed using PC1 and PC2 as input variables, outcome of the FPCA
393 conducted on the model-derived profiles. PC3 is not included to avoid implying a
394 seasonal water warming in the regime discrimination. An optimal number of four
395 clusters is given by the ICL criterion. After running the model-based clustering 100
396 times, two distinct patterns emerged. We selected the main pattern, occurring in
397 68 % of cases and presenting low variability in the cluster composition. The FODs
398 are then defined as groups containing profiles with a high probability of belonging
399 to a given cluster. The threshold is arbitrarily fixed at 0.75. This step leads to the
400 distinction of a fifth group composed of profiles with a probability lower than 0.75
401 and referred to as indeterminate profiles. Regimes 1 (purple), 2 (blue), 3 (green), 4
402 (yellow) and 5 (indeterminate) contain respectively 5.7 %, 18.4 %, 40.1 %, 24.2 %

403 and 11.6 % of the profiles considered over the 95 days. The proportions of the five
404 regimes vary over time as shown in Figure 5, with a notable gradual disappearance
405 of the first FOD (purple). The first FOD corresponds to cold and fresh waters with
406 little vertical variability between profiles as seen by the shade around the mean profile
407 (purple profiles, Figure 6a). The second FOD shows similar features to the first
408 group, with waters warmer above 80 m, slightly colder deeper, and saltier above
409 100 m (blue profiles). The FOD numbered 4 corresponds to hot and salty waters
410 with a high variability (yellow profiles), matching features of the BC. Finally, the
411 third FOD corresponds to intermediate features with high variability decreasing with
412 depth (green profiles, Figure 6a). This regime corresponds to waters that are formed
413 by the mixture of Subantarctic and Subtropical waters. The spatial distribution of
414 the clustering for the first day of the considered period is displayed in Figure 6b.
415 Regimes obtained show very consistent spatial and temporal patterns. Hot and salty
416 waters (yellow) form a coherent mass in the north part of the map, while the blue
417 and purple FODs follow the Patagonian slope. The green regime occupies a vast area
418 in the southeast part but with an indefinite shape. For both the yellow and green
419 FODs, the daily probability density function of PC1 shifts toward positive values (see
420 Supplementary Material), meaning that inside those regimes, the whole water column
421 cools down and gets fresher over time (corroborating the observed drop in the daily
422 trends, Figure 4). Gray filaments appear in Figure 6b and contain indeterminate
423 profiles. They mainly correspond to spatial transitions between the different regimes
424 and are considered as frontal zones.

425 3.3 Habitats used and foraging strategies

426 In situ profiles reaching 450 m depth account for 45.07 % of the total SES dives. Out
427 of this dataset, 4 463 are attributed to the day-time period, while 767 are attributed
428 to the night-time period. The remaining profiles occur either during the twilight
429 period or are not geolocalized.

430 Figure 7 shows the projection of the in situ profiles superimposed onto the 2D mapping
431 of the FPCA obtained from model-derived profiles. The marginal distributions reveal
432 high-density modes and the high concentration of model-derived observations in the
433 top right corner. The distribution of in situ TS profiles is pointed out by the 2D
434 density estimation (red to yellow lines). Each in situ profile is assigned to one of

435 the five regimes (considering indeterminate profiles) based on their coordinates on
436 the first factorial map (Figure 7). Figure 8 shows the five SES trajectories colored
437 according to the FOD and the proportion of regimes visited by the five females. The
438 spatial overlap of dives belonging to different FODs is explained by the displacement
439 of regimes in space over time. Indeterminate profiles occupy a notable part of the
440 trajectories (between 14 % and 25 %). All females except one visited the five regimes
441 but at different percentages. The yellow FOD is not always seen on the trajectories
442 meaning that this regime was visited by the females after the GPS stopped (i.e. the
443 dives are not geolocalized). Since the analyses do not rely on the location and time of
444 the profiles, it is indeed possible to assign a oceanographic regime to a non-localized
445 SES dive. The female named 2018-46 quickly crosses the purple and blue FODs and
446 spends a large part of her journey in the third regime identified (green). The other
447 females linger more in the cold waters associated with regimes one and two (purple
448 and blue), but are also found in the yellow regime, crossing highly contrasting waters
449 along their trips (Figure 6a). The passage between two FODs with opposite features
450 is sometimes performed in less than 24 hours (personal observations).

451 With the aim of understanding the SES habitat-visited proportions observed in Fig-
452 ure 8, the foraging strategy is studied within the scope of the FODs. The female
453 identified as 2018-47 can not be included in the foraging analysis as data from the
454 accelerometer is unavailable. Surprisingly, the foraging performances assessed by the
455 prey-capture rate (PCR) of the seals do not show much variation according to the
456 oceanographic regime (see Supplementary Material). At night, only the yellow regime
457 shows a slight decrease in PCR. During the day, the PCR is lower in the green regime
458 and slightly higher in the blue. The indeterminate group, corresponding to fronts
459 between FODs, do not imply significant changes in the PCR in comparison with the
460 other regimes. While the SES feed continuously along their pathways, the females
461 studied seem to favor the area where the different FODs meet and mix, at around 41° S
462 56° W (Figure 8). Dives are gathered in this zone in particular as the speed decreases
463 and the curvature increases (personal observations). To validate this assumption, a
464 criterion is created to reveal areas of high spatial and temporal oceanographic vari-
465 ability (Figure 9). This criterion is determined by calculating, for a given pixel, the
466 proportion of days (over the considered time-period) where the oceanographic domain
467 changes from a given day to the previous one. The spatial distribution of this criterion

468 is presented in [Figure 9](#). The map highlights one particular area with high probabili-
469 ties of having oceanographic conditions changing at day+1. This area corresponds to
470 the meeting of the FODs. Yellow filaments are seen along the Patagonian slope and
471 correspond to the displacement of the blue FOD over time, gradually substituting the
472 purple regime. Other areas of large probabilities are also observed in the northeastern
473 and southern parts of the map, and can be associated with frontal regions induced
474 by mesoscale features like the displacement of eddies carrying Subtropical waters in
475 the area. The probability value is extracted for each SES dive location and related
476 to the associated PCR. [Figure 10](#) depicts the relationship between the PCR and the
477 probability of changing regimes. The non-parametric regressions on the quantiles (Oh
478 et al., 2011; Simonoff, 2012) reveal a positive relation between the two variables even
479 if the data variability is high. The capture rate increases sharply to 0.15 with a slight
480 acceleration for the high percentiles. A small decrease arises around 0.2, then the
481 PCR gently increases with high probabilities. The median capture rate (red line) is
482 multiplied by 3.78, going from 3.5 capture per hour to 13.24. This result supports
483 the assumption that SES favor areas at the interface between water masses, where
484 they increase their foraging success.

485 4 Discussion

486 In this study, we aim to understand the habitat use of five elephant seals equipped in
487 2018 in Argentina, and the influence of oceanographic conditions on their foraging
488 strategies using descriptive statistics.

489 A functional principal component analysis followed by model-based clustering is used
490 to describe the Malvinas-Brazil Confluence at a regional scale. The multivariate
491 FPCA is an objective method developed in the oceanographic domain by Pauthenet
492 et al. (2017) to identify the thermohaline modes of the Southern Ocean. This ap-
493 proach presents strong potential as it not only allows the description of oceanographic
494 patterns at a global scale (Pauthenet et al., 2019) but also the definition of water-
495 mass boundaries and variability (Pauthenet et al., 2018). The analysis extracts the
496 principal modes of variability that describe and summarize the 3D thermohaline envi-
497 ronment through joint variations in temperature and salinity. Modes of variability are
498 orthogonal, considered as independent from each other. This multivariate technique

499 is extremely efficient in data reduction. The dataset used in this study is composed
500 of more than 1.5 million combinations of temperature and salinity profiles, with each
501 profile decomposed into 44 discrete values from 20 m to 450 m. We first projected
502 the model-derived profiles onto a B-spline basis with a small number K of functions.
503 Then, we worked on the two first principal components of the FPCA, which summa-
504 rize 98 % of the curve's shape variability. The B-spline basis used can not capture
505 the fine-scale variations of in situ profiles. Yet, since these profiles are projected into
506 the first factorial map of the clean and smooth model-derived profiles (Section 2.2.4),
507 the variations missed by the curve reconstruction do not impact the results in the
508 oceanographic regime attribution. Furthermore, smoothing the profiles with a small
509 number of basis functions is useful when data is potentially corrupted by noise, such
510 as in the case of in situ profiles (Nerini et al., 2010). The functional approach is
511 interesting because it integrates the vertical continuity of the data (considering the
512 inherent link between two consecutive values), working on curve shape decomposi-
513 tion. Moreover, curve reconstruction allows reducing the dimension of the data while
514 preserving the complexity of the curve shape. However, one constraint of the anal-
515 ysis is the requirement of equal depth range for each profile. Choice of the 450 m
516 threshold was motivated by the desire to take into account a large part of the water
517 column used by the SES. This limitation implies the removal of all profiles that do
518 not reach that depth, resulting in the elimination of the continental shelf area. As
519 females preferentially use the deep ocean basin (Campagna et al., 2021), this loss of
520 area has limited consequences. The 450 m threshold also implies the loss of many
521 night dives as these mostly do not reach that depth. Results on the foraging behavior
522 observed in this study are thus mainly driven by daylight dives and deep night dives,
523 necessitating cautious interpretation. One way to resolve this issue could be to recon-
524 struct the missing part of shallow profiles by functional methods. This solution would
525 allow consideration of a larger portion of night dives and could highlight potential
526 nighttime foraging variabilities between FODs that were missed out in this study.

527 Results of the FPCA applied to model-derived TS profiles demonstrate the method's
528 high capacity to decompose the BMC's main modes of variability. The three princi-
529 pal modes of vertical variability express the three main drivers of the oceanographic
530 conditions in this area at that period, namely: (1) a positional mode (PC1) depict-
531 ing the main vertical variability driven by the opposite features of the Brazil (north)

532 and Malvinas (south) Currents; (2) a dynamical mode (PC2) highlighting mesoscale
533 structures inherent to the confluence of the two currents; and (3) a seasonal mode
534 (PC3) revealing the spring to summer surface heating independent of the water's
535 origin. Moreover, as the method is applied over 95 days, it allows us to follow each
536 mode of vertical variability in space and time, giving key information about physical
537 processes occurring in the area (Figure 4). The trends of the daily mean and associ-
538 ated standard deviation of PC1 and PC2 can be associated with seasonal oscillations
539 and variability in Subantarctic and Subtropical influxes in the region but may also
540 indicate sporadic events that change the average thermohaline features in the region.

541 The model-based clustering applied on the first two principal components of the
542 FPCA led to the distinction of four FODs, whose thermohaline features share a
543 common vertical structure. A FOD can be considered as an assemblage of water
544 masses, integrating the vertical structure of the water column. The T-S diagram
545 (see Supplementary Material) indicates the water-mass composition of each FOD,
546 following definitions given by Gordon (1981), Maamaatuaiahutapu et al. (1994) and
547 Piola and Gordon (1989). The spatial coherence of the FODs obtained and their
548 consistency over time confirm the robustness of the analysis. The vertical features
549 of the fourth group (yellow) correspond to Subtropical waters transported by the
550 BC (Piola et al., 2001; Valla et al., 2018). In the upper layer of the yellow FOD,
551 we find the warmest and saltiest Tropical Waters (TW) above the South Atlantic
552 Central Waters (SACW, $\sigma_\theta < 27 \text{ kg m}^{-3}$) corresponding with the nearly straight line
553 in the diagram. The BC has been described as a high variability current (Valla et al.,
554 2018), corroborated in this study by a large interquartile vertical domain (Figure 6a).
555 This regime varies over time. The entire water column gets colder and fresher during
556 the considered period, suggesting a greater influx of Subantarctic waters within the
557 study area, while surface heating occurs (shown by the PC3). The third FOD (green)
558 corresponds to mixed waters resulting from the confluence of the BC and the MC,
559 as seen by the vertical features on the T-S diagram (see Supplementary Material).
560 These mixed waters occupy almost half of the considered area. The first and second
561 regimes (purple and blue) correspond to the Malvinas Current signatures (Piola et al.,
562 2001). The two groups have very similar vertical characteristics. They gather cold
563 and fresh profiles with low intra-cluster variability. The upper 100 m are composed of
564 Subantarctic Surface Waters (temperature $> 5 \text{ }^\circ\text{C}$, salinity $\sim 34 \text{ psu}$) while two water

565 masses are found deeper: the Subantarctic Mode Waters (temperature $\sim 5^\circ\text{C}$, salinity
566 ~ 34.2 psu) and Antarctic Intermediate Waters (temperature $< 4^\circ\text{C}$, salinity < 34.2
567 psu) (see Supplementary Material). The MC is the only current to carry Subantarctic
568 waters to Subtropical latitudes (Paniagua et al., 2021). It is generally accepted that
569 the MC starts at 55°S , follows the SAF and meets with the BC at approximately 38°
570 S (Artana et al., 2016), which corresponds to our observations (Figure 6b). The first
571 FOD (purple) corresponds to pure Subantarctic waters transported by the MC while
572 the second FOD (blue) may correspond to Subantarctic waters that have undergone
573 some mixing with Subtropical waters and are carried southward, up to 49°S , by
574 the Malvinas Return Current (MRC) (Saraceno et al., 2004). As the second regime
575 substitutes the first FOD over time (Figure 5), it indicates that the waters along
576 the Patagonian slope become colder under 100 meters depth, warmer above that
577 threshold and saltier above 150 meters depth. This observation is consistent with the
578 findings of Aubone et al. (2021) who studied the behavioral response of an elephant
579 seal staying over a small portion of the Patagonian slope to vertical thermohaline
580 variability of the MC. While the MC and the MRC are not distinguishable by an
581 analysis performed on TS surface data (not shown), the functional analysis applied
582 in this study succeeded in differentiating subtle patterns. In this way, the FODs
583 obtained in this study are slightly different from those obtained by Tournier et al.
584 (2021) who also performed a FDA to study the influence of oceanographic features on
585 mid-trophic levels through active acoustics, and found three oceanographic regimes
586 using SES in situ data. Features of those regimes are similar to the ones found in the
587 present study but they did not differentiate the MRC and the MC, probably due to
588 the clustering method and the use of selected in situ data to describe the thermohaline
589 environment instead of model-derived data as in our case.

590 Different approaches have been explored to determine biogeographical regions in the
591 BMC area but mostly using ocean surface variables from satellites (Gonzalez-Silvera
592 et al., 2004; Saraceno et al., 2006; Saraceno et al., 2005). An extension of our work
593 could comprise in integrating biogeochemical data like chlorophyll-*a* surface concen-
594 tration with TS functional data in clustering, and comparing the results with previous
595 findings. In other areas, different studies have also experimented with applying the
596 model-based clustering framework to temperature and/or salinity profiles to iden-
597 tify spatial oceanographic patterns (Maze, Mercier, and Cabanes, 2017). However,

598 most of these studies did not combine a functional approach with a Gaussian mixture
599 model (GMM), although this approach was suggested by Jones et al. (2019). The
600 GMM was applied in the North Atlantic and the SO using temperature profiles from
601 Argo floats (Jones et al., 2019; Maze, Mercier, Fablet, et al., 2017). More recently,
602 other studies have used profile classification model (PCM) in the multivariate case
603 to define regimes by their thermohaline structure (Boehme and Rosso, 2021; Rosso
604 et al., 2020). Although they all reduce the dimensionality of the data using a classical
605 principal component analysis, they do not preserve the original nature of the data
606 (i.e. the functional properties). The eigenvalue decomposition of a matrix \mathbf{T} in a
607 classical PCA remains invariant under the permutation of columns or rows. How-
608 ever, a permutation of the values in a profile (i.e. the columns of matrix \mathbf{T}) changes
609 the shape of the profile. Only a few papers leverage the functional properties of TS
610 profiles to define oceanographic regions. For instance, Assunção et al. (2020) ap-
611 plied two distinct FPCAs to temperature and salinity profiles and used a functional
612 hierarchical clustering to characterise the thermohaline structure of the Southwest-
613 ern tropical Atlantic. Here, our results demonstrate the potential and effectiveness
614 of combining multivariate FPCA and model-based clustering to extract key verti-
615 cal thermohaline features and identify oceanographic domains. This functional data
616 clustering approach falls under the category of *filtering methods* described in Jacques
617 and Preda (2014a). This category encompasses clustering on either basis coefficients
618 (James and Sugar, 2003) or on FPCA scores (Jacques and Preda, 2013, 2014b). Over
619 the last decades, a vast amount of literature has been produced on methodological
620 aspects and applications of the combination of FDA and clustering (Chamroukhi and
621 Nguyen, 2019; Jacques and Preda, 2014a; Wang et al., 2016; Zhang and Parnell,
622 2023). Some studies have expanded hierarchical clustering and k-means partitioning
623 methods to functional data (Abraham et al., 2003; Tokushige et al., 2007), while oth-
624 ers have focused on functional clustering using mixture models (Korte-Stapff et al.,
625 2022; Li et al., 2016; Schmutz et al., 2020). In the field of oceanography and lim-
626 nology, while the application of functional data clustering may appear limited in the
627 literature, functional data analysis has received more attention. Various studies are
628 moving toward functional models (FM) to explain or predict biological variables with
629 hydrological parameters (Ainsworth et al., 2011; Boudreault et al., 2021; Yen et al.,
630 2015). It is possible within the frame of FDA to use functions as responses and/or

631 predictor variables in regression models (Ramsay and Silverman, 2005). Considering
632 data as curves prevents information loss, improving models (Boudreault et al., 2021).
633 Bayle et al. (2015) demonstrated the ability of FM to predict vertical chlorophyll-*a*
634 from light profiles in the Antarctic region. Godard et al. (2020) have also shown that
635 functional analysis helps to deepen the understanding of animal behavior as their
636 study of SES dive shape allowed them to determine different dive patterns associated
637 with foraging success. The FDA framework was recently extended to the acoustic do-
638 main (Ariza et al., 2022), showing promising results for improving our understanding
639 of the links between oceanographic conditions and the structuring of sound-scattering
640 layers.

641 Model-based clustering also offers the advantage of allowing for uncertainty regarding
642 clustering (Bouveyron et al., 2019). In this present study, profiles with a probability
643 of belonging to a cluster under 0.75 form frontal filaments (gray color, Figure 6b),
644 which are in good agreement with intense fronts obtained with other criteria like
645 thermal gradients or with the Finite Size Lyapunov Exponents criterion (d'Ovidio et
646 al., 2010). The convergence of the MC and the BC with very different thermohaline
647 characteristics leads to energetic mixing processes and intrusions of Subantarctic and
648 Subtropical waters (Piola et al., 2001). These mesoscale structures are seen with the
649 second mode of variability obtained by the FPCA (Figure 3b). The Atlantic portion
650 of the Patagonian Shelf is marked by a large continental shelf extending from 34° S to
651 55° S and between the coastline and the 200 m isobath, followed by a slope plunging to
652 6 000 m depth (Weatherall et al., 2015). Several studies suggest that the interaction
653 of the complex ocean topography with the MC flow generates upwellings along the
654 shelf-break (Matano and Palma, 2008; Miller et al., 2011) and is also a source of
655 mesoscale processes (Fu, 2006; Mason et al., 2017; Saraceno and Provost, 2012). The
656 interaction of the shelfbreak, the nutrient-rich Subantarctic waters transported by
657 the MC, and the complex physical processes induced by the BMC, contribute to the
658 high phytoplankton biomass observed (Acha et al., 2004; Garcia et al., 2008). Indeed,
659 this region is known for its high chlorophyll-*a* concentration during the austral spring
660 and summer (Lutz et al., 2010; Romero et al., 2006; Saraceno et al., 2005). These
661 conditions support the marine ecosystems in the region and sustain one of the most
662 important fisheries in the southern hemisphere (Bogazzi et al., 2005; Martinetto et
663 al., 2020; Rey and Huettmann, 2020). The confluence associated with shelf blooms

664 makes the Argentine Basin a particularly interesting area for large pinnipeds like the
665 SES, whose females mainly feed there (Campagna et al., 2021).

1
2
3 666 The combination of FPCA with model-based clustering allows us to contextualize
4
5 667 the environment in the foraging area of the elephant seals at the regional scale. The
6
7 668 oceanographic domains identified are considered as distinct physical habitats and
8
9 669 used to study conditions visited by the SES and their foraging strategies. By pro-
10
11 670 jecting in situ profiles on the factorial plan obtained from the FPCA performed with
12
13 671 model-derived data, we are able to match the conditions visited by the females with
14
15 672 the range of possibilities revealed by the analysis. We consider this approach to be
16
17 673 more robust than directly performing clustering on in situ data. In fact, since model-
18
19 674 based clustering can be sensitive to initialization, clustering the TS profiles from SES
20
21 675 without taking precautions could result in highly variable groupings. Our results
22
23 676 demonstrate that clustering over a large dataset (> 1.5 million observations) yields
24
25 677 to a stable model and provides more objective interpretations of the oceanographic
26
27 678 regimes visited by the seals. The results show that SES foraging within the BMC
28
29 679 tend to visit all FODs present in the study area but in unequal proportions (Fig-
30
31 680 ure 8). The results also show intervariability between the seals, which may indicate
32
33 681 individual preferences. The percentages of the visited habitats observed (Figure 8)
34
35 682 do not correspond to the spatial space occupied by the regimes (Figure 5). For ex-
36
37 683 ample, the third group (green), which represents more than 40 % of the area, is
38
39 684 proportionally less visited by the elephant seals. One major advantage of studying
40
41 685 TS profiles through FDA is that it gives information about oceanographic conditions
42
43 686 encountered with no need for spatial coordinates. The consideration of non-localized
44
45 687 dives is necessary, first of all, to obtain an objective overview of habitat use, but is
46
47 688 also useful for accessing information that could otherwise be missed. The results of
48
49 689 the case presented here indicate that study of SES data allows us to find the four
50
51 690 FODs observed at the regional scale. In this way, although our vision depends on
52
53 691 their trajectory choice, the five seals offer a representative picture of the area. The
54
55 692 decomposition of TS profiles through FPCA was also performed independently on in
56
57 693 situ profiles from the SES. The results were similar whether using in situ or Mercator
58
59 694 profiles (Table 1), confirming the representativeness of SES data. Furthermore, the
60
61 695 similarity of results indicates that while modeled profiles did not capture the thermo-
62
63 696 haline complexity of the water column (e.g. the profiles are relatively smooth), they
64
65

697 were efficient in finding the main oceanographic patterns in the region. The chosen
698 CMEMS product is a model derived from the Nucleus for European Modelling of the
699 Ocean (NEMO), which assimilates in situ temperature and salinity profiles. There-
700 fore, it is expected to be consistent with the recorded SES data. However, on any
701 given day, the TS model-derived profiles can be very different from those recorded by
702 the animal-borne device at the same geolocation. This phenomenon is particularly
703 noticeable in the area where all the regimes meet and mix. This comes as no surprise
704 as the model is not a perfect representation of reality and is likely to be less efficient
705 for locating water-mass boundaries precisely—information more accurately extracted
706 from the geolocalized in situ SES TS profiles.

707 The capture rate is used as a proxy of foraging success to investigate if the identified
708 FODs have an influence on SES habitat choices. We find that foraging performances
709 of the five SES studied are mostly unrelated to the visited regimes. The oligotrophic
710 waters advected by the BC leads to a slight decrease in PCR during the night but
711 not during the day. This can be explained by prey availability being affected by the
712 warm waters of the epipelagic layer. The daily PCR is slightly higher in the blue
713 FOD, which may indicate a nutrient input associated with the Malvinas Return Cur-
714 rent and impacting higher trophic levels (Aubone et al., 2021). To better understand
715 SES foraging strategies, we took advantage of the model-based clustering analysis
716 to create a criterion of physical-condition variability by computing the probability
717 of changing regimes. Interestingly, we found that foraging performance is associated
718 with the probability of changing FODs (Figure 10), regardless of the specific FOD.
719 The median prey-catch rate (PCR) is nearly quadrupled when there is a 50 % prob-
720 ability of changing FOD the following day. The background gray dots in Figure 10
721 illustrate a high variability in PCR, but all quantile regressions exhibit the same in-
722 creasing trend. Our study suggests that instead of selecting a particular regime, SES
723 may look for areas of high oceanographic variability found at the interface between
724 FODs. This result is consistent with previous findings highlighting the importance
725 of oceanographic fronts and eddies on movement behavior and foraging performances
726 of SES (Bailleul et al., 2010; Cotté et al., 2015; Della Penna et al., 2015; Dragon
727 et al., 2010; Rivière et al., 2019). However, the indeterminate group resulting from
728 the model-based clustering and corresponding to frontal areas between FODs, do not
729 imply a PCR increase although it represents a large part of the group proportion

730 (Figure 8 and Supplementary Material). This may indicate that only some particular
731 frontal areas attract and are favored by SES. For more extensive studies, Lagrangian
732 approaches may be complementary to comprehensively understand frontal-system im-
733 pacts (Baudena et al., 2021; Bon et al., 2015). Finally, drawing general assumptions
734 about the habitat use and foraging strategies of elephant seals based on only five
735 individuals requires caution. To validate our findings regarding elephant seals' be-
736 havior in the Argentine Basin, it would be beneficial to incorporate a larger number
737 of individuals in future studies.

738 5 Conclusion

739 Technological advances of the last decades have led to massive deployments of ocean-
740 observing systems recording environmental variables at a very high frequency and
741 accuracy. The huge datasets that result from such sensors need statistical tools to
742 extract the main information and analyze the data integrating their complexity. In
743 this paper, we explored functional data analysis combining model-derived data and
744 in situ data collected from southern elephant seals (SES). Our results confirm the
745 adequacy of using functional approaches for computing large and complex datasets.
746 This framework followed by model-based clustering was appropriate for describing the
747 foraging environment of five SES in 2018 and helping to understand their habitat
748 use. New loggers, such as a head-mounted microsonar, should provide fine-scale
749 insight into variations in the density of midtrophic level (MTL) organisms (i.e. macro-
750 zooplankton and micronekton) that could explain variability in elephant seal foraging
751 behavior. On the basis of our current findings, we hypothesize that the greatest
752 densities of MTL organisms are likely to be found at the interface between Functional
753 Oceanographic Domains (FOD) rather than within specific FODs. Functional data
754 analyses are promising methods for advancing study of the interaction between SES
755 behavior, MTL organisms (including preys of SES) and environmental conditions.

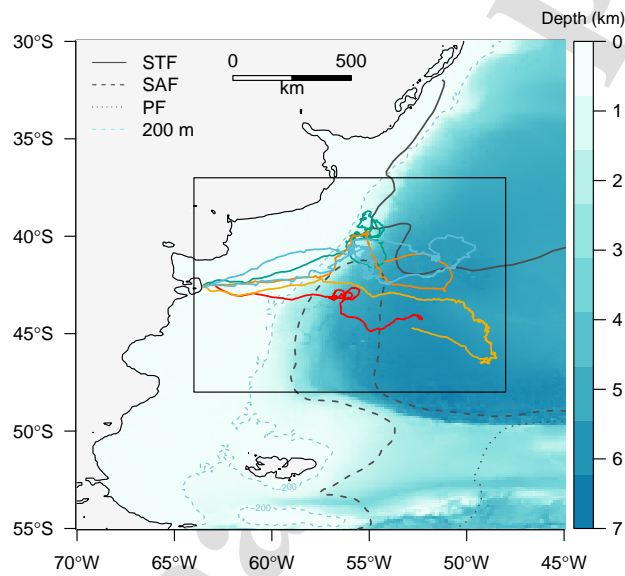
756 Declaration of competing interest

757 None.

758 Acknowledgments

1 759 Through NF Ph.D, this work was funded by the French Ministry for Education and
 2
 3 760 Research. We thank all people that have been involved in the fieldwork in Argentina
 4
 5 761 (Península Valdés), part of the SABIO French-Argentinian collaborative program
 6
 7 762 (PI Christophe Guinet and Martin Saraceno) supported by CNES-TOSCA (Centre
 8
 9 763 National d'Etudes Spatiales). We also thank Mark Johnson for providing the tags, Fui
 10
 11 764 Lee Luk for english correction, and Lloyd Izard for his advices and personal support.

765 Table and figures



45
 46 **Figure 1:** Colored trajectories represent the five SES females equipped in October
 47 2018 at Península Valdés and used for the analysis. The black rectangle defines the
 48 focus area. Black lines delimit the Subtropical Front (STF), the Subantarctic Front
 49 (SAF) and the Polar Front (PF) from Orsi et al. (1995). The blue color gradient
 50 indicates the bathymetry, and the 200 m isobath (blue dashed line) defines the limit
 51 between the continental shelf and the slope.
 52

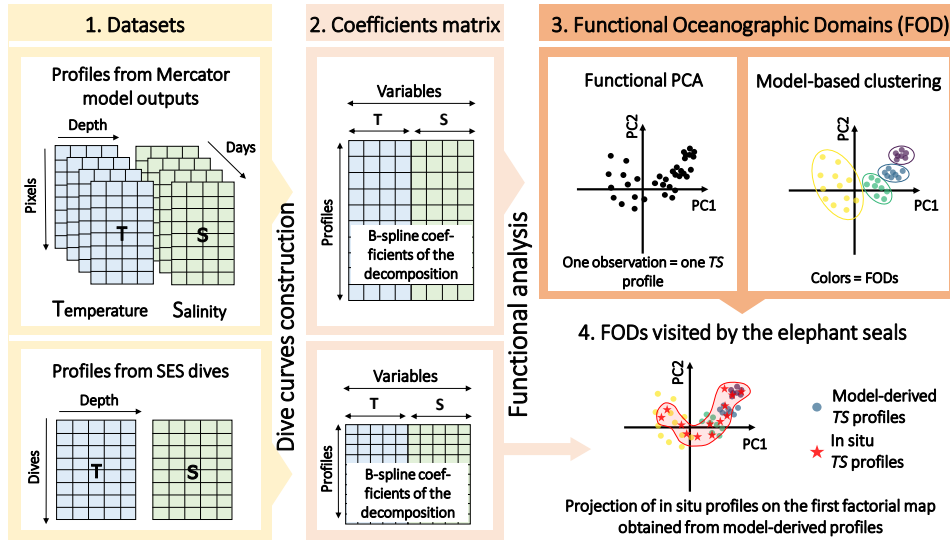


Figure 2: Workflow of the functional analysis. (1) Model-derived and in situ TS profiles are stored in different data frames. (2). TS profiles are approximated with continuous curves described by the coefficients of the B-spline decomposition. The coefficients are stored in new matrices. Each row corresponds to one observation. (3) The model-derived observations are decomposed into modes of variability with the FPCA and projected onto a space of reduce dimension. Model-based clustering is performed in the space of the first principal components to identify FODs (i.e. regimes sharing similar oceanographic structure). Steps (2) and (3) reduce the dimensionality of the initial data. (4) Finally, in situ observations from elephant seals are projected onto the factorial map as new statistical observations to associate each dive with one FOD and determine the habitat visited by the SES.

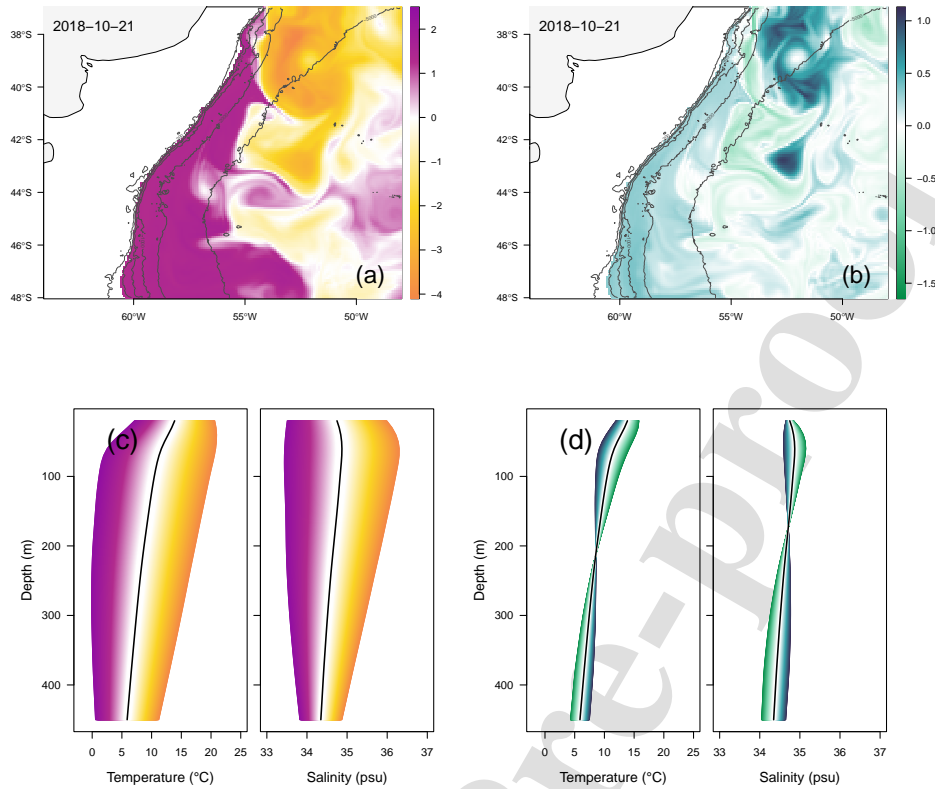


Figure 3: (a,b) Spatial distribution of the first and second PCs for 21 October 2018. Colors indicate the magnitude of the scores and match with color gradients in (c) and (d). The pink, orange, blue and green areas correspond with temperature and salinity profiles in pink, orange, blue and green (respectively) seen in (c). PC1 highlights the contrast between the BC (hot and salty) and the MC (cold and fresh), while PC2 reveals coherent mesoscale patterns. Bathymetry lines at 200, 500, 700, 1 000, 2 000 and 5 000 m define the Patagonian slope. (c,d) Vertical shapes induced by the first two eigenfunctions (respectively). The color gradients represent the effect of adding or subtracting (respectively pink or orange in (c), blue or green in (d)) each mode with a magnitude of two (see Pauthenet et al., 2017, for more details). The black line indicates the mean profile, and represents the center of gravity of the factorial map seen in Figure 7.

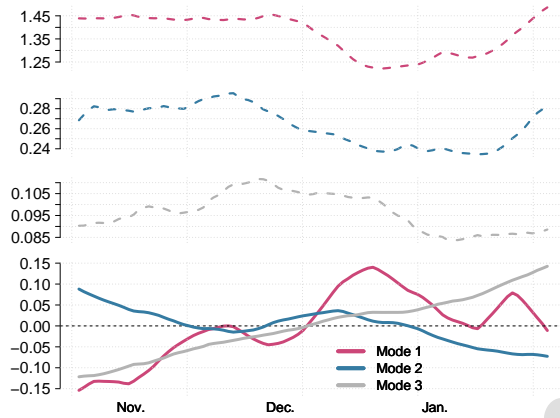


Figure 4: Trends of the daily mean (continuous lines) and associated daily standard deviation (dashed lines) for PC1 (pink), PC2 (blue) and PC3 (gray).

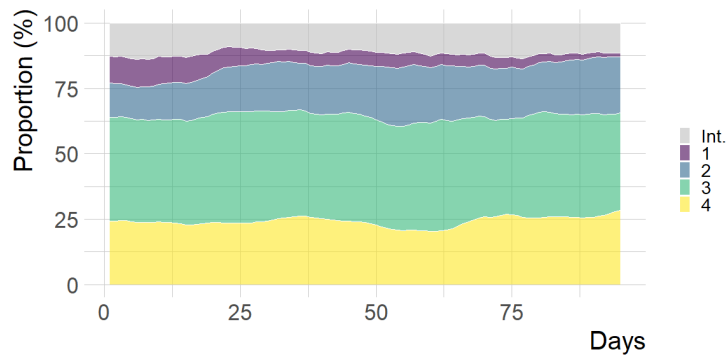


Figure 5: Proportion (%) occupied by the FODs in the considered area over the 95 days (21 October 2018 to 23 January 2019). The colors refer to the 4 FODs with the gray part corresponding to indeterminate profiles (Int.).

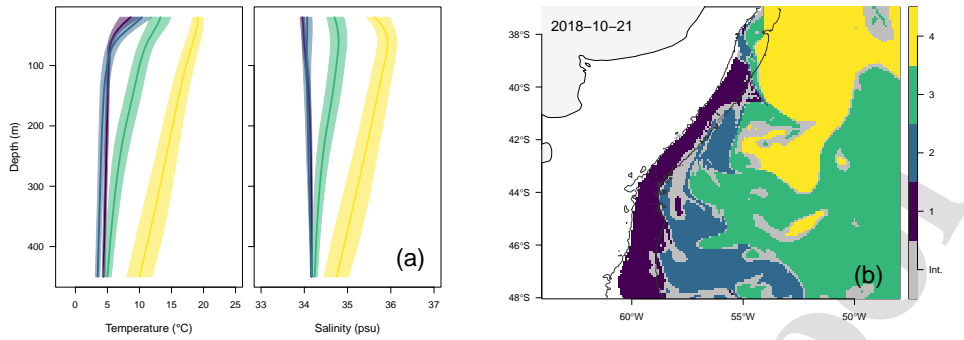


Figure 6: (a) Mean temperature and salinity profiles (solid lines) associated with the FODs obtained from the clustering (after removing profiles with a probability < 0.75). Regimes are colored in purple (cluster 1), blue (cluster 2), green (cluster 3) and yellow (cluster 4). The envelopes contain 50 % of the profiles, delimiting the first and third quartiles calculated for each cluster. (b) Spatial distribution of the five regimes on 21 October 2018. The colors match with the profiles in (a). Profiles with a probability < 0.75 of belonging to a group are colored in gray and form filaments between the regimes. Bathymetry lines at 200 and 2 000 m are drawn.

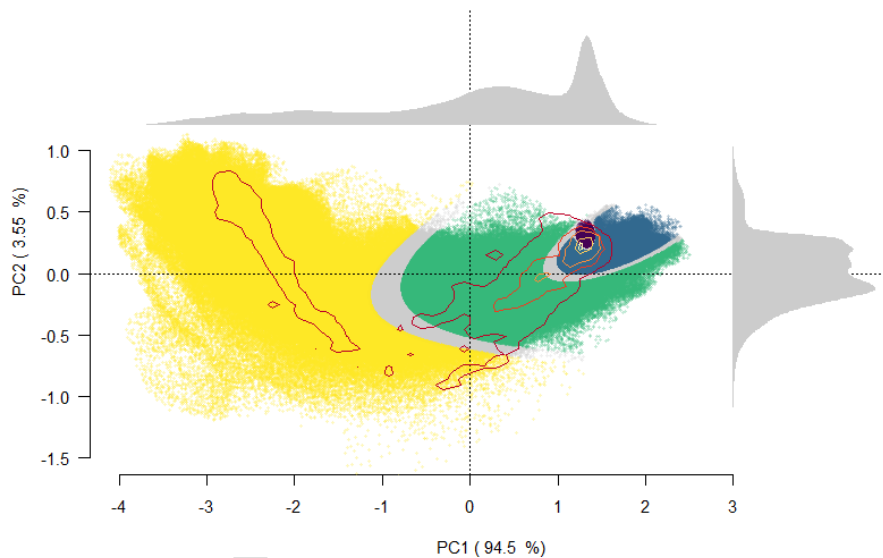


Figure 7: First factorial map of the functional PCA performed on model-derived data (colored dots) and clustering results. Gray dots correspond to observations with a probability of belonging to a cluster under 0.75. Marginal density probability of the first and second principal components are drawn (gray densities on the upper and right sides). They show modes of high density indicating areas of high concentrated model-derived observations. The 2D kernel density estimation (red to yellow lines) displays the projection of SES in situ TS profiles. The increasingly lighter successive lines contain respectively 2.5, 25, 50, 75 and 97.5 % of the dives centered around local density maximums. Each SES dive is associated to a FOD or to the indeterminate profiles group (gray).

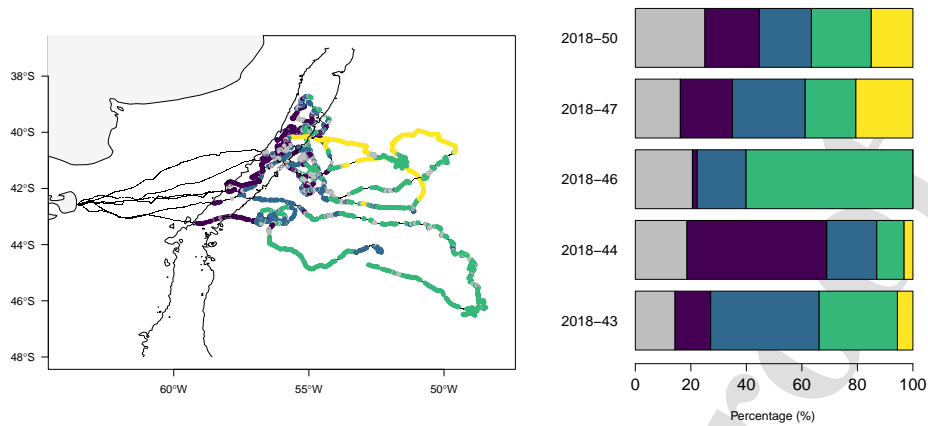


Figure 8: Trajectories of the five females colored according to the FODs identified and proportion of dives belonging to each regime including indeterminate profiles (gray group). Numbers 2018-43 to 50 correspond to SES identification. Refer to [Figure 6](#) for FOD features and names. Bathymetry lines at 200 and 2 000 m are drawn.

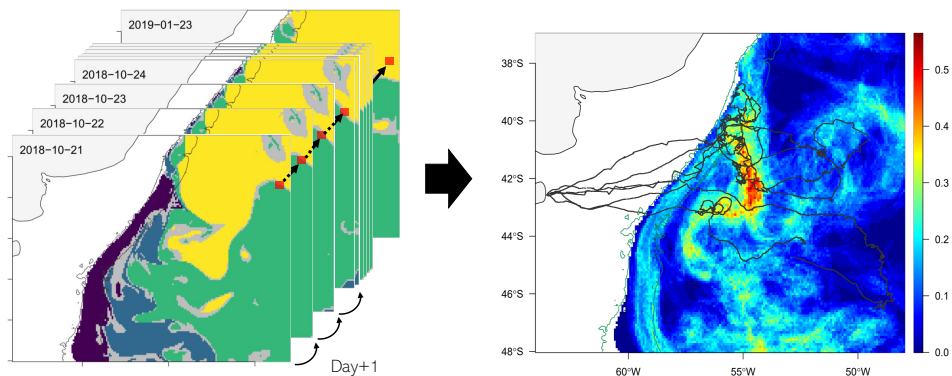


Figure 9: Probability of changing regimes at day+1. For a given pixel (red square), the proportion of days where the oceanographic regime change from a day to the next one is calculated (see the schematic view on the left). High probability values are colored in red and highlight a high variability area in the center of the map (right panel).

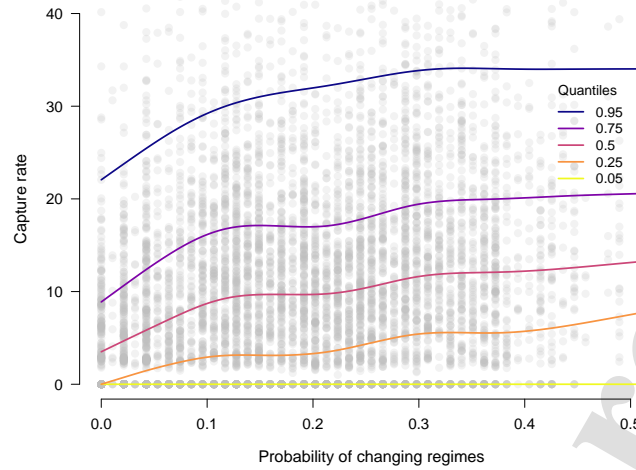


Figure 10: Scatter plot of prey-capture rate (captures per hour) against probability of changing regimes extracted for each SES dive. The lines indicate the non-parametric quantile regression at the quantiles of order 0.05, 0.25, 0.5, 0.75 and 0.95 respectively. For example, the red line corresponds to the median prey-capture rate and shows an increase from 3.5 to 13.24 captures per hour, which corresponds to a multiplication factor of 3.78, as the probability increases from 0 to 0.5.

Table 1: Variance (%) explained by the first principal components obtained from the functional PCA performed on model-derived and in situ profiles.

	Principal components		
	PC1	PC2	PC2
ACPF with model-derived TS profiles	94.50 %	3.55 %	0.72 %
ACPF with <i>in situ</i> TS profiles	88.14 %	5.93 %	1.98 %

References

- Abraham, C., Cornillon, P.-A., Matzner-Løber, E., & Molinari, N. (2003). Unsupervised curve clustering using b-splines. *Scandinavian journal of statistics*, *30*(3), 581–595.
- Acha, E. M., Mianzan, H. W., Guerrero, R. A., Favero, M., & Bava, J. (2004). Marine fronts at the continental shelves of austral south america: Physical and ecological processes. *Journal of Marine systems*, *44*(1-2), 83–105.

- 773 Ainsworth, L., Routledge, R., & Cao, J. (2011). Functional data analysis in ecosystem
774 research: The decline of oweekeno lake sockeye salmon and wannock river flow.
775 *Journal of agricultural, biological, and environmental statistics*, *16*(2), 282–
776 300.
- 777 Ariza, A., Lengaigne, M., Menkes, C., Lebourges-Dhaussy, A., Receveur, A., Gorgues,
778 T., Habasque, J., Gutiérrez, M., Maury, O., & Bertrand, A. (2022). Global
779 decline of pelagic fauna in a warmer ocean. *Nature Climate Change*, *12*(10),
780 928–934.
- 781 Artana, C., Ferrari, R., Koenig, Z., Saraceno, M., Piola, A. R., & Provost, C. (2016).
782 Malvinas current variability from argo floats and satellite altimetry. *Journal*
783 *of Geophysical Research: Oceans*, *121*(7), 4854–4872.
- 784 Assunção, R. V., Silva, A. C., Roy, A., Bourlès, B., Silva, C. H. S., Ternon, J.-F.,
785 Araujo, M., & Bertrand, A. (2020). 3d characterisation of the thermohaline
786 structure in the southwestern tropical atlantic derived from functional data
787 analysis of in situ profiles. *Progress in Oceanography*, *187*, 102399.
- 788 Aubone, N., Saraceno, M., Alberto, M. T., Campagna, J., Le Ster, L., Picard, B.,
789 Hindell, M., Campagna, C., & Guinet, C. (2021). Physical changes recorded
790 by a deep diving seal on the patagonian slope drive large ecological changes.
791 *Journal of Marine Systems*, *223*, 103612.
- 792 Bailleul, F., Vacquie-Garcia, J., & Guinet, C. (2015). Dissolved oxygen sensor in
793 animal-borne instruments: An innovation for monitoring the health of oceans
794 and investigating the functioning of marine ecosystems. *PLoS One*, *10*(7),
795 e0132681.
- 796 Bailleul, F., Cotté, C., & Guinet, C. (2010). Mesoscale eddies as foraging area of
797 a deep-diving predator, the southern elephant seal. *Marine Ecology Progress*
798 *Series*, *408*, 251–264.
- 799 Baudena, A., Ser-Giacomi, E., D’Onofrio, D., Capet, X., Cotté, C., Cherel, Y., &
800 D’Ovidio, F. (2021). Fine-scale structures as spots of increased fish concentra-
801 tion in the open ocean. *Scientific Reports*, *11*(1), 1–13.
- 802 Bayle, S., Monestiez, P., Guinet, C., & Nerini, D. (2015). Moving toward finer scales
803 in oceanography: Predictive linear functional model of chlorophyll a profile
804 from light data. *Progress in Oceanography*, *134*, 221–231.

- 805 Biernacki, C., Celeux, G., & Govaert, G. (2000). Assessing a mixture model for clus-
806 tering with the integrated completed likelihood. *IEEE transactions on pattern*
807 *analysis and machine intelligence*, 22(7), 719–725.
- 808 Block, B. A., Holbrook, C. M., Simmons, S. E., Holland, K. N., Ault, J. S., Costa,
809 D. P., Mate, B. R., Seitz, A. C., Arendt, M. D., Payne, J. C., et al. (2016).
810 Toward a national animal telemetry network for aquatic observations in the
811 united states. *Animal Biotelemetry*, 4(1), 1–8.
- 812 Block, B. A., Jonsen, I. D., Jorgensen, S. J., Winship, A. J., Shaffer, S. A., Bograd,
813 S. J., Hazen, E. L., Foley, D. G., Breed, G., Harrison, A.-L., et al. (2011). Track-
814 ing apex marine predator movements in a dynamic ocean. *Nature*, 475(7354),
815 86–90.
- 816 Boehme, L., & Rosso, I. (2021). Classifying oceanographic structures in the amundsen
817 sea, antarctica. *Geophysical Research Letters*, 48(5), e2020GL089412.
- 818 Boehme, L., Thompson, D., Fedak, M., Bowen, D., Hammill, M. O., & Stenson, G. B.
819 (2012). How many seals were there? the global shelf loss during the last glacial
820 maximum and its effect on the size and distribution of grey seal populations.
821 *Plos one*, 7(12), e53000.
- 822 Bogazzi, E., Baldoni, A., Rivas, A., Martos, P., Reta, R., Orensanz, J. M., Lasta, M.,
823 Dell’Arciprete, P., & Werner, F. (2005). Spatial correspondence between areas
824 of concentration of patagonian scallop (*zygochlamys patagonica*) and frontal
825 systems in the southwestern atlantic. *Fisheries Oceanography*, 14(5), 359–376.
- 826 Bon, C., Della Penna, A., d’Ovidio, F., YP Arnould, J., Poupart, T., & Bost, C.-A.
827 (2015). Influence of oceanographic structures on foraging strategies: Macaroni
828 penguins at crozet islands. *Movement ecology*, 3(1), 1–11.
- 829 Boudreault, J., St-Hilaire, A., Chebana, F., & Bergeron, N. E. (2021). Modelling
830 fish physico-thermal habitat selection using functional regression. *Journal of*
831 *Ecohydraulics*, 6(2), 105–120.
- 832 Bouveyron, C., Celeux, G., Murphy, T. B., & Raftery, A. E. (2019). *Model-based*
833 *clustering and classification for data science: With applications in r* (Vol. 50).
834 Cambridge University Press.
- 835 Campagna, C., Piola, A. R., Marin, M. R., Lewis, M., & Fernández, T. (2006). South-
836 ern elephant seal trajectories, fronts and eddies in the brazil/malvinas conflu-

- 837 ence. *Deep Sea Research Part I: Oceanographic Research Papers*, 53(12), 1907–
838 1924.
- 1
2 839 Campagna, J., Lewis, M. N., González Carman, V., Campagna, C., Guinet, C., John-
3 son, M., Davis, R. W., Rodriguez, D. H., & Hindell, M. A. (2021). Ontogenetic
4 840 niche partitioning in southern elephant seals from argentine patagonia. *Marine*
5 *Mammal Science*, 37(2), 631–651.
6 841
7 842
8
9 843 Carse, F., Martin, M. J., Sellar, A., & Blockley, E. W. (2015). Impact of assim-
10 ilating temperature and salinity measurements by animal-borne sensors on
11 844 foam ocean model fields. *Quarterly Journal of the Royal Meteorological Soci-*
12 *ety*, 141(693), 2934–2943.
13 845
14 846
15 847 Chamroukhi, F., & Nguyen, H. D. (2019). Model-based clustering and classification of
16 functional data. *Wiley Interdisciplinary Reviews: Data Mining and Knowledge*
17 *Discovery*, 9(4), e1298.
18 848
19 849
20
21 850 Chelton, D. B., Schlax, M. G., Witter, D. L., & Richman, J. G. (1990). Geosat
22 altimeter observations of the surface circulation of the southern ocean. *Journal*
23 *of Geophysical Research: Oceans*, 95(C10), 17877–17903.
24 851
25 852
26
27 853 Conn, P. B., Thorson, J. T., & Johnson, D. S. (2017). Confronting preferential sam-
28 pling when analysing population distributions: Diagnosis and model-based
29 trriage. *Methods in Ecology and Evolution*, 8(11), 1535–1546.
30 854
31 855
32 856 Cotté, C., d'Ovidio, F., Dragon, A.-C., Guinet, C., & Lévy, M. (2015). Flexible pref-
33 erence of southern elephant seals for distinct mesoscale features within the
34 antarctic circumpolar current. *Progress in Oceanography*, 131, 46–58.
35 857
36 858
37 859 Cuevas, A. (2014). A partial overview of the theory of statistics with functional data.
38 *Journal of Statistical Planning and Inference*, 147, 1–23.
39 860
40 861 Deacon, G. E. R. (1937). The hydrology of the southern ocean. *Discovery Rep.*, 15,
41 3–122.
42 862
43 863 Della Penna, A., De Monte, S., Kestenare, E., Guinet, C., & d'Ovidio, F. (2015).
44 Quasi-planktonic behavior of foraging top marine predators. *Scientific reports*,
45 5(1), 1–10.
46 864
47 865
48 866 Dinsdale, D., & Salibian-Barrera, M. (2019). Modelling ocean temperatures from bio-
49 probes under preferential sampling.
50
51
52
53
54
55
56
57
58
59
60
61
62
63
64
65

- 868 d'Ovidio, F., De Monte, S., Alvain, S., Dandonneau, Y., & Lévy, M. (2010). Fluid
869 dynamical niches of phytoplankton types. *Proceedings of the National Academy
870 of Sciences*, 107(43), 18366–18370.
- 871 Dragon, A.-C., Monestiez, P., Bar-Hen, A., & Guinet, C. (2010). Linking foraging
872 behaviour to physical oceanographic structures: Southern elephant seals and
873 mesoscale eddies east of kerguelen islands. *Progress in Oceanography*, 87(1-4),
874 61–71.
- 875 Evans, K., Lea, M.-A., & Patterson, T. (2013). Recent advances in bio-logging science:
876 Technologies and methods for understanding animal behaviour and physiology
877 and their environments.
- 878 Fedak, M., et al. (2004). Marine animals as platforms for oceanographic sampling: A”
879 win/win” situation for biology and operational oceanography.
- 880 Fedak, M. (2013). The impact of animal platforms on polar ocean observation. *Deep
881 Sea Research Part II: Topical Studies in Oceanography*, 88, 7–13.
- 882 Fraley, C., & Raftery, A. E. (2002). Model-based clustering, discriminant analysis, and
883 density estimation. *Journal of the American statistical Association*, 97(458),
884 611–631.
- 885 Fu, L.-L. (2006). Pathways of eddies in the south atlantic ocean revealed from satellite
886 altimeter observations. *Geophysical Research Letters*, 33(14).
- 887 Gallon, S., Bailleul, F., Charrassin, J.-B., Guinet, C., Bost, C.-A., Handrich, Y., &
888 Hindell, M. (2013). Identifying foraging events in deep diving southern ele-
889 phant seals, *mirounga leonina*, using acceleration data loggers. *Deep Sea Re-
890 search Part II: Topical Studies in Oceanography*, 88, 14–22.
- 891 Garcia, V. M., Garcia, C. A., Mata, M. M., Pollery, R. C., Piola, A. R., Signorini,
892 S. R., McClain, C. R., & Iglesias-Rodriguez, M. D. (2008). Environmental
893 factors controlling the phytoplankton blooms at the patagonia shelf-break
894 in spring. *Deep Sea Research Part I: Oceanographic Research Papers*, 55(9),
895 1150–1166.
- 896 Godard, M., Manté, C., Guinet, C., Picard, B., & Nerini, D. (2020). Diving behavior
897 of *mirounga leonina*: A functional data analysis approach. *Frontiers in Marine
898 Science*, 7, 595.
- 899 Gonzalez-Silvera, A., Santamaria-del-Angel, E., Garcia, V. M., Garcia, C. A., Millán-
900 Nuñez, R., & Muller-Karger, F. (2004). Biogeographical regions of the tropical

- 901 and subtropical atlantic ocean off south america: Classification based on pig-
902 ment (czcs) and chlorophyll-a (seawifs) variability. *Continental Shelf Research*,
903 *24*(9), 983–1000.
- 904 Gordon, A. L. (1981). South atlantic thermocline ventilation. *Deep Sea Research Part*
905 *A. Oceanographic Research Papers*, *28*(11), 1239–1264.
- 906 Goulet, P., Guinet, C., Campagna, C., Campagna, J., Tyack, P. L., & Johnson,
907 M. (2020). Flash and grab: Deep-diving southern elephant seals trigger anti-
908 predator flashes in bioluminescent prey. *Journal of Experimental Biology*, *223*(10),
909 jeb222810.
- 910 Goulet, P., Guinet, C., Swift, R., Madsen, P. T., & Johnson, M. (2019). A minia-
911 ture biomimetic sonar and movement tag to study the biotic environment
912 and predator-prey interactions in aquatic animals. *Deep Sea Research Part I:*
913 *Oceanographic Research Papers*, *148*, 1–11.
- 914 Guinet, C., Vacquié-Garcia, J., Picard, B., Bessigneul, G., Lebras, Y., Dragon, A. C.,
915 Viviant, M., Arnould, J. P., & Bailleul, F. (2014). Southern elephant seal
916 foraging success in relation to temperature and light conditions: Insight into
917 prey distribution. *Marine Ecology Progress Series*, *499*, 285–301.
- 918 Harcourt, R., Sequeira, A. M., Zhang, X., Roquet, F., Komatsu, K., Heupel, M.,
919 McMahon, C., Whoriskey, F., Meekan, M., Carroll, G., et al. (2019). Animal-
920 borne telemetry: An integral component of the ocean observing toolkit. *Frontiers in Marine Science*, *6*, 326.
- 922 Hays, G. C., Ferreira, L. C., Sequeira, A. M., Meekan, M. G., Duarte, C. M., Bailey,
923 H., Bailleul, F., Bowen, W. D., Caley, M. J., Costa, D. P., et al. (2016).
924 Key questions in marine megafauna movement ecology. *Trends in ecology &*
925 *evolution*, *31*(6), 463–475.
- 926 Hindell, M. A., McMahon, C. R., Bester, M. N., Boehme, L., Costa, D., Fedak, M. A.,
927 Guinet, C., Herraiz-Borreguero, L., Harcourt, R. G., Huckstadt, L., et al.
928 (2016). Circumpolar habitat use in the southern elephant seal: Implications
929 for foraging success and population trajectories. *Ecosphere*, *7*(5), e01213.
- 930 Hindell, M. A., Reisinger, R. R., Ropert-Coudert, Y., Hückstädt, L. A., Trathan, P. N.,
931 Bornemann, H., Charrassin, J.-B., Chown, S. L., Costa, D. P., Danis, B., et al.
932 (2020). Tracking of marine predators to protect southern ocean ecosystems.
933 *Nature*, *580*(7801), 87–92.

- 934 Hussey, N. E., Kessel, S. T., Aarestrup, K., Cooke, S. J., Cowley, P. D., Fisk, A. T.,
935 Harcourt, R. G., Holland, K. N., Iverson, S. J., Kocik, J. F., et al. (2015).
936 Aquatic animal telemetry: A panoramic window into the underwater world.
937 *Science*, *348*(6240), 1255642.
- 938 Jacques, J., & Preda, C. (2013). Funclust: A curves clustering method using functional
939 random variables density approximation. *Neurocomputing*, *112*, 164–171.
- 940 Jacques, J., & Preda, C. (2014a). Functional data clustering: A survey. *Advances in*
941 *Data Analysis and Classification*, *8*, 231–255.
- 942 Jacques, J., & Preda, C. (2014b). Model-based clustering for multivariate functional
943 data. *Computational Statistics & Data Analysis*, *71*, 92–106.
- 944 James, G. M., & Sugar, C. A. (2003). Clustering for sparsely sampled functional data.
945 *Journal of the American Statistical Association*, *98*(462), 397–408.
- 946 Jaud, T., Dragon, A.-C., Garcia, J. V., & Guinet, C. (2012). Relationship between
947 chlorophyll a concentration, light attenuation and diving depth of the southern
948 elephant seal *mirounga leonina*.
- 949 Jones, D. C., Holt, H. J., Meijers, A. J., & Shuckburgh, E. (2019). Unsupervised cluster-
950 ing of southern ocean argo float temperature profiles. *Journal of Geophysical*
951 *Research: Oceans*, *124*(1), 390–402.
- 952 Jonsen, I. D., Myers, R. A., & James, M. C. (2007). Identifying leatherback turtle for-
953 aging behaviour from satellite telemetry using a switching state-space model.
954 *Marine Ecology Progress Series*, *337*, 255–264.
- 955 Jouma'a, J., Le Bras, Y., Richard, G., Vacquié-Garcia, J., Picard, B., El Ksabi, N.,
956 & Guinet, C. (2016). Adjustment of diving behaviour with prey encounters
957 and body condition in a deep diving predator: The southern elephant seal.
958 *Functional Ecology*, *30*(4), 636–648.
- 959 Korte-Stapff, M., Yarger, D., Stoev, S., & Hsing, T. (2022). A multivariate functional-
960 data mixture model for spatio-temporal data: Inference and cokriging. *arXiv*
961 *preprint arXiv:2211.04012*.
- 962 Labrousse, S., Williams, G., Tamura, T., Bestley, S., Sallée, J.-B., Fraser, A. D.,
963 Sumner, M., Roquet, F., Heerah, K., Picard, B., et al. (2018). Coastal polynyas:
964 Winter oases for subadult southern elephant seals in east antarctica. *Scientific*
965 *Reports*, *8*(1), 1–15.

- 966 Le Bras, Y., Jouma'a, J., & Guinet, C. (2017). Three-dimensional space use during
 967 the bottom phase of southern elephant seal dives. *Movement ecology*, 5(1),
 968 1–15.
- 969 Le Bras, Y., Jouma'a, J., Picard, B., & Guinet, C. (2016). How elephant seals (mirounga
 970 leonina) adjust their fine scale horizontal movement and diving behaviour in
 971 relation to prey encounter rate. *PLoS One*, 11(12), e0167226.
- 972 Li, H., Deng, X., Dolloff, C. A., & Smith, E. P. (2016). Bivariate functional data
 973 clustering: Grouping streams based on a varying coefficient model of the stream
 974 water and air temperature relationship. *Environmetrics*, 27(1), 15–26.
- 975 Lopez, R., Malardé, J.-P., Danès, P., & Gaspar, P. (2015). Improving argos doppler
 976 location using multiple-model smoothing. *Animal Biotelemetry*, 3(1), 1–9.
- 977 Lutz, V. A., Segura, V., Dogliotti, A. I., Gagliardini, D. A., Bianchi, A. A., &
 978 Balestrini, C. F. (2010). Primary production in the argentine sea during spring
 979 estimated by field and satellite models. *Journal of Plankton Research*, 32(2),
 980 181–195.
- 981 Maamaatuaiahutapu, K., Garçon, V. C., Provost, C., Boulahdid, M., & Bianchi, A. A.
 982 (1994). Spring and winter water mass composition in the brazil-malvinas con-
 983 fluence. *Journal of Marine Research*, 52(3), 397–426.
- 984 March, D., Boehme, L., Tintoré, J., Vélez-Belchi, P. J., & Godley, B. J. (2020). To-
 985 wards the integration of animal-borne instruments into global ocean observing
 986 systems. *Global change biology*, 26(2), 586–596.
- 987 Martinetto, P., Alemany, D., Botto, F., Mastrángelo, M., Falabella, V., Acha, E. M.,
 988 Antón, G., Bianchi, A., Campagna, C., Cañete, G., et al. (2020). Linking the
 989 scientific knowledge on marine frontal systems with ecosystem services. *Ambio*,
 990 49(2), 541–556.
- 991 Mason, E., Pascual, A., Gaube, P., Ruiz, S., Pelegrí, J. L., & Delepoulle, A. (2017).
 992 Subregional characterization of mesoscale eddies across the brazil-malvinas
 993 confluence. *Journal of Geophysical Research: Oceans*, 122(4), 3329–3357.
- 994 Matano, R. P., & Palma, E. D. (2008). On the upwelling of downwelling currents.
 995 *Journal of Physical Oceanography*, 38(11), 2482–2500.
- 996 Maze, G., Mercier, H., & Cabanes, C. (2017). Profile classification models. *Mercator
 997 Ocean Journal*, (55), 48–56.

- 998 Maze, G., Mercier, H., Fablet, R., Tandeo, P., Radcenco, M. L., Lenca, P., Feucher,
 999 C., & Le Goff, C. (2017). Coherent heat patterns revealed by unsupervised
 1000 classification of argo temperature profiles in the north atlantic ocean. *Progress*
 1001 *in Oceanography*, 151, 275–292.
- 1002 McMahon, C. R., Field, I. C., Bradshaw, C. J., White, G. C., & Hindell, M. A. (2008).
 1003 Tracking and data-logging devices attached to elephant seals do not affect
 1004 individual mass gain or survival. *Journal of Experimental Marine Biology and*
 1005 *Ecology*, 360(2), 71–77.
- 1006 McMahon, C. R., Roquet, F., Baudel, S., Belbeoch, M., Bestley, S., Blight, C.,
 1007 Boehme, L., Carse, F., Costa, D. P., Fedak, M. A., et al. (2021). Animal borne
 1008 ocean sensors—anibos—an essential component of the global ocean observing
 1009 system. *Frontiers in Marine Science*, 1625.
- 1010 Miller, R. N., Matano, R. P., & Palma, E. D. (2011). Shelfbreak upwelling induced
 1011 by alongshore currents: Analytical and numerical results. *Journal of Fluid*
 1012 *Mechanics*, 686, 239–249.
- 1013 Nerini, D., Manté, C., & Monestiez, P. (2022). Extending functional kriging when
 1014 data are multivariate curves: Some technical considerations and operational
 1015 solutions. *Geostatistical Functional Data Analysis*, 73–103.
- 1016 Nerini, D., Monestiez, P., & Manté, C. (2010). Cokriging for spatial functional data.
 1017 *Journal of Multivariate Analysis*, 101(2), 409–418.
- 1018 Oh, H.-S., Lee, T. C., & Nychka, D. W. (2011). Fast nonparametric quantile regression
 1019 with arbitrary smoothing methods. *Journal of Computational and Graphical*
 1020 *Statistics*, 20(2), 510–526.
- 1021 Orsi, A. H., Whitworth III, T., & Nowlin Jr, W. D. (1995). On the meridional extent
 1022 and fronts of the antarctic circumpolar current. *Deep Sea Research Part I:*
 1023 *Oceanographic Research Papers*, 42(5), 641–673.
- 1024 Paniagua, G. F., Saraceno, M., Piola, A. R., Charo, M., Ferrari, R., Artana, C., &
 1025 Provost, C. (2021). Malvinas current at 44.7° s: First assessment of velocity
 1026 temporal variability from in situ data. *Progress in Oceanography*, 195, 102592.
- 1027 Pauthenet, E., Roquet, F., Madec, G., Guinet, C., Hindell, M., Memahon, C. R.,
 1028 Harcourt, R., & Nerini, D. (2018). Seasonal meandering of the polar front
 1029 upstream of the kerguelen plateau. *Geophysical Research Letters*, 45(18), 9774–
 1030 9781.

- 1031 Pauthenet, E., Roquet, F., Madec, G., & Nerini, D. (2017). A linear decomposition of
1032 the southern ocean thermohaline structure. *Journal of Physical Oceanography*,
1033 47(1), 29–47.
- 1034 Pauthenet, E., Roquet, F., Madec, G., Sallée, J.-B., & Nerini, D. (2019). The thermo-
1035 haline modes of the global ocean. *Journal of Physical Oceanography*, 49(10),
1036 2535–2552.
- 1037 Payne, N. L., Meyer, C. G., Smith, J. A., Houghton, J. D., Barnett, A., Holmes,
1038 B. J., Nakamura, I., Papastamatiou, Y. P., Royer, M. A., Coffey, D. M., et al.
1039 (2018). Combining abundance and performance data reveals how temperature
1040 regulates coastal occurrences and activity of a roaming apex predator. *Global*
1041 *change biology*, 24(5), 1884–1893.
- 1042 Piola, A. R., & Gordon, A. L. (1989). Intermediate waters in the southwest south
1043 atlantic. *Deep Sea Research Part A. Oceanographic Research Papers*, 36(1),
1044 1–16.
- 1045 Piola, A., & Falabella, V. (2009). El mar patagónico (2009) atlas del mar patagónico:
1046 Especies y espacios. *Wildlife Conservation Society and Birdlife International*,
1047 *Buenos Aires*, 56–75.
- 1048 Piola, A., Matano, R., Steele, J., Thorpe, S., & Turekian, K. (2001). Brazil and
1049 falklands (malvinas) currents. *Ocean currents*, 35–43.
- 1050 Ramsay, J. O. (1982). When the data are functions. *Psychometrika*, 47(4), 379–396.
- 1051 Ramsay, J. O., & Silverman, B. W. (2005). *Functional data analysis*. Springer 2nd
1052 Edn. New York, NY.
- 1053 Ramsay, J., Hooker, G., & Graves, S. (2009). Introduction to functional data analysis.
1054 In *Functional data analysis with r and matlab* (pp. 1–19). Springer.
- 1055 Rey, A. R., & Huettmann, F. (2020). Telecoupling analysis of the patagonian shelf:
1056 A new approach to study global seabird-fisheries interactions to achieve sus-
1057 tainability. *Journal for Nature Conservation*, 53, 125748.
- 1058 Rivière, P., Jaud, T., Siegelman, L., Klein, P., Cotté, C., Le Sommer, J., Dencausse,
1059 G., & Guinet, C. (2019). Sub-mesoscale fronts modify elephant seals foraging
1060 behavior. *Limnology and Oceanography Letters*, 4(6), 193–204.
- 1061 Romero, S. I., Piola, A. R., Charo, M., & Garcia, C. A. E. (2006). Chlorophyll-a vari-
1062 ability off patagonia based on seawifs data. *Journal of Geophysical Research:*
1063 *Oceans*, 111(C5).

- 1064 Roquet, F., Charrassin, J.-B., Marchand, S., Boehme, L., Fedak, M., Reverdin, G.,
1065 & Guinet, C. (2011). Delayed-mode calibration of hydrographic data obtained
1066 from animal-borne satellite relay data loggers. *Journal of Atmospheric and*
1067 *Oceanic Technology*, 28(6), 787–801.
- 1068 Roquet, F., Williams, G., Hindell, M. A., Harcourt, R., McMahon, C., Guinet, C.,
1069 Charrassin, J.-B., Reverdin, G., Boehme, L., Lovell, P., et al. (2014). A south-
1070 ern indian ocean database of hydrographic profiles obtained with instrumented
1071 elephant seals. *Scientific data*, 1(1), 1–10.
- 1072 Roquet, F., Wunsch, C., Forget, G., Heimbach, P., Guinet, C., Reverdin, G., Char-
1073 rassin, J.-B., Bailleul, F., Costa, D. P., Huckstadt, L. A., et al. (2013). Es-
1074 timates of the southern ocean general circulation improved by animal-borne
1075 instruments. *Geophysical Research Letters*, 40(23), 6176–6180.
- 1076 Rosso, I., Mazloff, M. R., Talley, L. D., Purkey, S. G., Freeman, N. M., & Maze,
1077 G. (2020). Water mass and biogeochemical variability in the kerguelen sector
1078 of the southern ocean: A machine learning approach for a mixing hot spot.
1079 *Journal of Geophysical Research: Oceans*, 125(3), e2019JC015877.
- 1080 Saraceno, M., & Provost, C. (2012). On eddy polarity distribution in the southwestern
1081 atlantic. *Deep Sea Research Part I: Oceanographic Research Papers*, 69, 62–69.
- 1082 Saraceno, M., Provost, C., & Lebbah, M. (2006). Biophysical regions identification
1083 using an artificial neuronal network: A case study in the south western atlantic.
1084 *Advances in Space Research*, 37(4), 793–805.
- 1085 Saraceno, M., Provost, C., & Piola, A. R. (2005). On the relationship between satellite-
1086 retrieved surface temperature fronts and chlorophyll a in the western south
1087 atlantic. *Journal of Geophysical Research: Oceans*, 110(C11).
- 1088 Saraceno, M., Provost, C., Piola, A. R., Bava, J., & Gagliardini, A. (2004). Brazil
1089 malvinas frontal system as seen from 9 years of advanced very high resolution
1090 radiometer data. *Journal of Geophysical Research: Oceans*, 109(C5).
- 1091 Schmutz, A., Jacques, J., Bouveyron, C., Cheze, L., & Martin, P. (2020). Clustering
1092 multivariate functional data in group-specific functional subspaces. *Computa-
1093 tional Statistics*, 35(3), 1101–1131.
- 1094 Schreer, J. F., & Kovacs, K. M. (1997). Allometry of diving capacity in air-breathing
1095 vertebrates. *Canadian Journal of Zoology*, 75(3), 339–358.

- 1096 Schwarz, G. (1978). Estimating the dimension of a model. *The annals of statistics*,
1097 461–464.
- 1 1098 Scrucca, L., Fop, M., Murphy, T. B., & Raftery, A. E. (2016). Mclust 5: Clustering,
2 3 classification and density estimation using gaussian finite mixture models. *The*
4 1099 *R journal*, 8(1), 289.
- 5 1100
6 1101 Siegelman, L., O’toole, M., Flexas, M., Rivière, P., & Klein, P. (2019). Submesoscale
7 8 ocean fronts act as biological hotspot for southern elephant seal. *Scientific*
9 1102 *reports*, 9(1), 1–13.
- 10 1103
11 1104 Simonoff, J. S. (2012). *Smoothing methods in statistics*. Springer Science & Business
12 13 Media.
- 14 1105
15 1106 Team, R. C. (2021). R: A language and environment for statistical computing (r
16 17 version 4.0.3, r foundation for statistical computing, vienna, austria, 2020).
18 1107
19 1108 *Google Scholar There is no corresponding record for this reference.*
- 20 1109 Tokushige, S., Yadohisa, H., & Inada, K. (2007). Crisp and fuzzy k-means clustering
21 22 algorithms for multivariate functional data. *Computational Statistics*, 22, 1–
23 24 16.
- 25 1110
26 1111
27 1112 Tournier, M., Goulet, P., Fonville, N., Nerini, D., Johnson, M., & Guinet, C. (2021).
28 1113 A novel animal-borne miniature echosounder to observe the distribution and
29 30 migration patterns of intermediate trophic levels in the southern ocean. *Jour-*
31 1114 *nal of Marine Systems*, 223, 103608.
- 32 1115
33 1116 Ullah, S., & Finch, C. F. (2013). Applications of functional data analysis: A systematic
34 35 review. *BMC medical research methodology*, 13, 1–12.
- 36 1117
37 1118 Vacquie-Garcia, J., Royer, F., Dragon, A.-C., Viviant, M., Bailleul, F., & Guinet, C.
38 1119 (2012). Foraging in the darkness of the southern ocean: Influence of biolumi-
39 40 nescence on a deep diving predator.
- 41 1120
42 1121 Valla, D., Piola, A. R., Meinen, C. S., & Campos, E. (2018). Strong mixing and recir-
43 44 culation in the northwestern argentine basin. *Journal of Geophysical Research:*
45 1122 *Oceans*, 123(7), 4624–4648.
- 46 1123
47 1124 Viviant, M., Trites, A. W., Rosen, D. A., Monestiez, P., & Guinet, C. (2010). Prey
48 49 capture attempts can be detected in steller sea lions and other marine preda-
50 51 tors using accelerometers. *Polar biology*, 33(5), 713–719.
- 52 1125
53 1126
54 1127 Wahba, G. (1990). *Spline models for observational data*. SIAM.
- 55 56
57 58
59 60
61 62
63 64
65

- 1128 Wang, J.-L., Chiou, J.-M., & Müller, H.-G. (2016). Functional data analysis. *Annual*
1129 *Review of Statistics and its application*, 3, 257–295.
- 1130 Weatherall, P., Marks, K. M., Jakobsson, M., Schmitt, T., Tani, S., Arndt, J. E.,
1131 Rovere, M., Chayes, D., Ferrini, V., & Wigley, R. (2015). A new digital bathy-
1132 metric model of the world’s oceans. *Earth and space Science*, 2(8), 331–345.
- 1133 Wolfe, J. H. (1963). *Object cluster analysis of social areas* (Doctoral dissertation).
1134 University of California.
- 1135 Wunsch, C., & Ferrari, R. (2004). Vertical mixing, energy, and the general circulation
1136 of the oceans. *Annual Review of Fluid Mechanics*, 36(1), 281–314.
- 1137 Yen, J. D., Thomson, J. R., Paganin, D. M., Keith, J. M., & Mac Nally, R. (2015).
1138 Function regression in ecology and evolution: Free. *Methods in Ecology and*
1139 *Evolution*, 6(1), 17–26.
- 1140 Zhang, M., & Parnell, A. (2023). Review of clustering methods for functional data.
1141 *ACM Transactions on Knowledge Discovery from Data*, 17(7), 1–34.

Highlights :

- Functional data analysis coupled with model-based clustering is a powerful method to identify oceanographic domains.
- Five functional oceanographic domains sharing similar thermohaline features are identified in the Brazil-Malvinas Confluence.
- Coupling data from model with in situ elephant seal profiles allows us to characterize habitats use by these predators.
- The studied elephant seals tend to visit all the oceanographic domains in varying proportion.
- The studied elephant seals increase their prey capture rate in transitions areas, i.e. where the probability of changing functional oceanographic domains is high.

Declaration of interests

The authors declare that they have no known competing financial interests or personal relationships that could have appeared to influence the work reported in this paper.

The authors declare the following financial interests/personal relationships which may be considered as potential competing interests:

Journal Pre-proof